AN ABSTRACT OF THE THESIS OF

Lexi Coons for the degree of Master of Science in Water Resource Science presented on

June 13, 2013

Title: Seeing the Snow through the Trees: Towards a Validated Canopy Adjustment for Satellite Fractional Snow-Covered Area

Abstract Approved: _____

Anne W. Nolin

Forest canopy cover presents a major challenge for remote sensing of fractional snow-covered area (fSCA). Snow cover is systematically underestimated where satellites sensors cannot penetrate the forest canopy. Current canopy adjustments scale observable fSCA with the vegetation fraction, assuming that snow cover distributions are similar between sub-canopy and open locations. This assumption may be invalid because snow accumulation and ablation processes depend on forest characteristics. This study addresses how individual trees and the forest canopy affect snow cover distributions with the goal of determining metrics that can characterize spatial patterns of sub-canopy snow cover. *In situ* snow cover and forest canopy measurements were made at several snow study sites in the Oregon Cascades. These were compared to canopy-adjusted satellite estimates of fSCA. Differences between *in situ* and satellite fSCA were assessed based

on forest canopy structure derived from manual surveys along transects, and 3-D terrestrial laser scanning (TLS). For larger spatial context, a simple geometric-optical model (SGM) was used to estimate forest canopy parameters from aerial photographs and multi-angular satellite data. The canopy adjustment resulted in improvements over unadjusted *f*SCA. However, a single canopy adjustment function is not able to adequately adjust for snow under trees in all cases. At the lower elevation sites, snow was present in the low-density forest sites for at least 14 days after it had completely disappeared from the high-density forested sites. At the higher elevation sites, snow remained in the high-density forested sites for at least 7 days after it had completely disappeared from the low-density sites. In assessing the vegetation survey results we found that TLS effectively depicted tree heights and crown radii, but the SGM estimates of canopy structure from aerial photographs and satellite multi-angular reflectance data require further refinement in dense forests before being applied for operational canopy adjustments.

Seeing the Snow through the Trees: Towards a Validated Canopy Adjustment for Satellite Fractional Snow-Covered Area

by

Lexi Coons

A THESIS

Submitted to

Oregon State University

in partial fulfillment of

the requirements for the

degree of

Master of Science

Presented June 13, 2013

Commencement June 2014

Master of Science thesis of Lexi Coons presented on June 13, 2013.

APPROVED:

Major Professor, representing Water Resource Science

Director of the Water Resources Graduate Program

Dean of the Graduate School

I understand that my thesis will become part of the permanent collection of Oregon State University libraries. My signature below authorizes release of my thesis to any reader upon request.

_____

Lexi Coons, Author

ACKNOWLEDGEMENTS

I would like to offer my sincere gratitude to Dr. Anne Nolin, who as my major advisor, provided tremendous support in the formation of this research project and was integral to my success in the Water Resource Graduate Program. I would also like to thank my committee members Dr. Julia Jones, Dr. Thomas Hilker, and Dr. Skip Rochefort for contributing knowledge and insight on the various stages of this work. I am grateful to Dr. Thomas Painter and Karl Rittger with the Jet Propulsion Laboratory for providing crucial remote sensing data and answering many questions on the details related to their work. Kelly Gleason and Travis Roth were extremely generous to share field data, Eugene Mar performed a great service in providing computing support for modeling above my realm of expertise, and the remainder of the Mountain Hydroclimatology Research Group offered much intellectual and moral support. Dr. Michael Olsen, John Raugust, Hamid Mahmoudabadi, and Rubini Santha in the Geomatics Research group contributed endless hours processing TLS data and troubleshooting data issues. I am indebted to the students and faculty in CEOAS and the Water Resources Graduate Program for providing support and constructive feedback during all stages of my academic career. Finally, this work would not have been possible without financial support from the MISR Science Team subcontract with the NASA Jet Propulsion Laboratory for NPP VIIRS. The NSF Water Sustainability and Climate Award, EAR-1039192 also provided support.

TABLE OF CONTENTS

TABLE OF CONTENTS (Continued)

LIST OF FIGURES

LIST OF FIGURES (continued)

LIST OF TABLES

Seeing the Snow through the Trees: Towards a Validated Canopy Adjustment for Satellite Fractional Snow-Covered Area

Chapter 1. Introduction

1.1. Motivation and research questions

A combination of snow driven hydrologic and climate processes make the accurate and timely monitoring of snow's spatial extent essential for many disciplines. Snowpacks serve as vital reservoirs of water, supplying human and ecosystem needs. Spring snowmelt contributes to soil moisture stores, recharges groundwater reservoirs, and augments streamflow. Seasonal decreases in snow-covered area (SCA), signal the initiation and duration of snowmelt runoff, so assimilation of this metric into hydrologic models provides an effective means of evaluating snow as a water resource [*Martinec and Rango*, 1995*; Clark et al*., 2006; *McGuire et al*., 2006; *Thirel et al*., 2011].

SCA is also an important variable driving climate models because the interplay between albedo and solar radiation in forested vs. open areas can create either a positive or negative feedback mechanism depending on the presence of snow [*Randerson et al*., 2006; *O'Halloran et al*., 2012; *Jin et al.,* 2012]. Extensive snow cover has a high albedo, which decreases the amount of absorbed solar radiation, contributes to cold surface temperatures, and allows snow cover to persist. When the snow is obscured by forest canopy the land surface albedo decreases significantly. Open, snow-free areas have low albedos, which absorb more solar radiation, warm surface temperatures. At the small scale, when snow-free areas are adjacent to snow-covered areas their warmer temperatures modify snowmelt rates and allow snow-free regions to propagate [Shook et al., 1993]. On a large scale, these mechanisms contribute to global climate patterns and will have bearing on the hydrologic responses to a changing climate [*Qu and Hall*, 2006; *Fletcher et al*., 2009].

Notable decreases to snow-covered area have occurred in North America during the past decade [*Mote*, 2006; *Brown and Mote*, 2009; *Abatzoglou*, 2011; *Pederson et al.*, 2013] and predictions suggest these trends will continue [*Nolin and Daly,* 2006; *Stoelinga et al*., 2010]. The hydrologic implications of these changes remain uncertain. Consequently, the demand for accurate SCA estimates will increase as global climate change alters the extent and duration of this water resource [*Mote et al*., 2005; *Dozier*, 2011*; Jefferson*, 2011].

Satellite remote sensing has the potential to meet such demand as spaceborne sensors can capture a large geographic extent of the Earth's surface. Active and passive satellite-based sensors can effectively detect snow and give estimates of SCA at various spatial and temporal resolutions [*Nolin,* 2010]. Recent advances in snow remote sensing have led to improved estimates of SCA by providing subpixel, or fractional snow-covered area (*f*SCA) [*Painter et al*., 2009]. An operational *f*SCA product, while still in the evaluation phase, will be available from a new satellite sensor, the Visible Infrared Imaging Radiometer Suite (VIIRS). This sensor, onboard NASA's recently launched Earth-observing satellite, will provide global estimates of *f*SCA as part of a mission to quantify and monitor the Earth's cryosphere and its response to climate change [*Baker*, 2011].

An obstacle to accurate mapping of snow-covered area occurs in forested areas. Forest canopy inhibits an accurate depiction of SCA because satellite sensors cannot detect sub-canopy snow [*Nolin*, 2010]. This issue has yet to be adequately addressed and the current canopy adjustment for *f*SCA in forests assumes that hidden, sub-canopy

*f*SCA mirrors detectable *f*SCA in canopy openings [*Raleigh et al*., 2013*; Rittger et al*., 2013]. This approach may be unjustified since forest canopy influences snow accumulation and ablation, causing spatial variability in the distribution of snow cover [*Golding and Swanson*, 1986; *Davis et al*., 1997; *Faria et al*., 2000; *Storck et al*., 2002; *Musselman et al*., 2008; *Varhola et al*., 2010; *Ellis et al*., 2011].

Despite numerous research efforts focused on the relationships between snow properties and forest characteristics [*Storck et al*., 2002; *Musselman et al*., 2008; *Varhola et al*., 2010; *Ellis et al.,* 2011], few studies [*Raleigh et al*., 2013; *Rittger et al*., 2013] have addressed how these relationships may be linked to satellite estimates of SCA. *Raleigh et al*. [2013] and *Rittger et al*. [2013] validated a simple forest canopy adjustment that uses fractional vegetation cover, but to date there has been no systematic assessment of snowpack spatial relationships with forest canopy structure at the scale of remote sensing pixels. An improved canopy adjustment requires identifying forest canopy metrics that can be used to parameterize sub-canopy snow at scales appropriate for remote sensing. With proper representation at an appropriate spatial resolution, these forest metrics will serve as valuable input to a canopy adjustment for satellite-derived SCA.

To understand the limitations of current canopy adjustments and progress towards a method to account for sub-canopy snow, this study aims to answer the following research questions: 1) How well do original satellite-derived *f*SCA and canopy adjusted *f*SCA approximate sub-canopy *f*SCA? 2) What spatio-temporal snow cover patterns explain differences between *in situ* snow cover and satellite-derived *f*SCA? 3) What canopy structure metrics can account for differences between snow cover and satellite-

derived *f*SCA? 4) What remote sensing techniques can be used to represent forest canopy structure at the landscape scale for future incorporation into a canopy adjustment?

1.2. Background and previous work

1.2.1. Remote sensing of snow cover

Methods for monitoring SCA include ground-based surveys, automated digital photography [*Hinkler*, 2002], airborne light detection and ranging (LiDAR) [*Hopkinson et al*., 2004b], and satellite remote sensing [*Dozier*, 1989; *Painter et al*., 2009]. Of these approaches, satellite remote sensing offers the most readily available and spatially extensive method for estimating SCA. Optical remote sensing from space can provide global coverage and some sensors deliver daily products of SCA. These benefits diminish the need for intensive *in situ* measurements or expensive aerial monitoring, and are especially advantageous in remote alpine environments [*Nolin*, 2010].

Satellite sensors that record land surface reflectance can effectively detect snow cover because its spectral "signature" makes it easily distinguishable from other surfaces [*Dozier*, 1989; *Dozier*, 2011]. *Dozier* [1989] established an automated method for detecting snow from satellite reflectance data. This method, the normalized difference snow index (NDSI), discriminates snow from other land surfaces by quantifying the contrast between reflectance values in the visible (R_{VIS}) and near infrared (R_{NIR}) portions of the electromagnetic spectrum [*Dozier*, 1989]:

$$NDSI = \frac{R_{VIS} - R_{NIR}}{R_{VIS} + R_{NIR}} \quad (1)$$

The resulting NDSI values are used to map image pixels as entirely snow-covered or snow-free, with an NDSI value greater than 0.4 typically indicating a snow-covered pixel [*Dozier*, 1989].

This binary snow mapping does not allow for mixed pixels that include portions of the ground surface that are only partially snow-covered [*Elder et al*., 1998]. The spatial resolution of sensors typically used to map snow, 30 m for Landsat [*Dozier*, 1989] and 500 m for MODIS [*Hall and Riggs*, 2007], cannot always capture the local-scale spatial variability of snow cover [*Elder et al.,* 1998; *Dozier et al.,* 2008; *Rittger et al.* 2013]. This spatial heterogeneity results from a number of factors including elevation, topography and vegetation [*Blöschl and Kirnbauer,* 1992; *Elder et al*., 1998; *Anderton*, 2004; *Trujillo et al*., 2007]. At low elevations, patchy snow cover occurs around the snow line where a transition from snow-free to snow-covered ground occurs [*Elder et al*., 1998; *Kerr et al*., 2013]. At high elevations, patchy snow cover can occur on steep topography where the slope angle is too high for snow to accumulate [*Kerr et al*., 2013]. Vegetation and micro-topography further influence snow cover by governing snow accumulation, melt, and wind redistribution [*Elder et al*., 1998; *Anderton*, 2004; *Trujillo et al*., 2007]. Moderate resolution binary snow products have a tendency to overestimate snow cover at high elevations and underestimate it at low elevations where these patchy conditions occur [*Dozier et al*., 2008].

Methods for mapping *f*SCA present the opportunity to better represent this sub-pixel heterogeneity of snow cover [*Molotch and Margulis*, 2008; *Rittger et al*., 2013]. The fractional product from NASA's Moderate Resolution Imaging SpectroRadiometer

(MODIS) is based on an empirical relationship between the NDSI and *f*SCA [*Salomonson and Appel*, 2004]. This fractional product does not show significant improvements over the binary snow product available from MODIS when compared to *f*SCA from the Landsat Enhanced Thematic Mapper (ETM+) [*Rittger et al*., 2013].

An alternative method for mapping *f*SCA uses spectral mixture analysis of reflectance data over a heterogeneous, snowy land surface. Spectral mixture analysis was first used for mapping snow-covered area by *Nolin et al.* [1993] and later refined by *Painter et al.* [2009] for operational use with MODIS data. The algorithm developed by *Painter et al*. [2009], called MODIS Snow-Covered Area and Grain size (MODSCAG), evaluates the spectral signatures of the different land cover types ("endmembers") contributing to total pixel reflectance. The result is a linear combination of fractional contributions from key endmembers: snow (including snow with different grain sizes), vegetation, and bare ground [*Painter et al*., 2009]:

$$R_{S,\lambda} = \sum_i f_i R_{\lambda,i} + \varepsilon_\lambda \quad (2)$$

Where $R_{s,\lambda}$ is the pixel-averaged reflectance from MODIS band λ, f_i is the fraction of each surface *i* (snow, vegetation, or bare ground), $R_{\lambda i}$ is the reflectance of each surface in λ, and ε_λ is the residual error for λ that provides the best fit of the linear combination. MODSCAG and the adapted algorithm for Landsat ETM+ (TMSCAG) can evaluate the reflectance in partially snow-covered pixels to return estimates of *f*SCA with a lower limit of 0.15 snow cover. Snow fractions below 0.15 are considered to be snow-free [*Painter et al*., 2009; *Rittger et al*., 2013].

Satellite estimates of SCA and *f*SCA act as valuable data used to constrain and drive hydrologic and snowmelt models. The spatial extent of snow given by satellite reflectance data can be used with snowmelt models to distribute snow water equivalent (SWE) measurements over large spatial extents [*Molotch and Margulis,* 2008]. Additionally, inputs of SCA have been included in several hydrologic models to improve predictions of basin runoff [*Lee et al.,* 2005; *Clark et al.,* 2006; *Thirel et al*., 2011] and streamflow forecasts for reservoir operations [*Martinec and Rango, 1995; McGuire et al.,* 2006]. The Snowmelt Runoff Model (SRM) is a simple conceptual model that relies on SCA and a degree-day factor to simulate runoff [*Martinec and Rango,* 1986]. This model has been used globally to effectively simulate historical streamflow [*Butt and Bilal,* 2011], make real time forecasts [*Martinec and Rango,* 1995], and more recently to simulate variations in streamflow as a result of changing climate [*Martinec and Rango,* 2008]. The accuracy of the SRM and utility of satellite-derived SCA for improving streamflow predictions from other hydrologic models depends on the accurate mapping and quantification of SCA [*Clark et al.,* 2006, *McGuire et al.,* 2006].

Dense forest canopy presents a limitation to all optical remote sensing techniques for detecting snow cover. The resulting systematic underestimation of *f*SCA poses a challenge for hydrologic and climate models that rely on accurate estimates of SCA because 40% of the North American seasonal snow zone is forested [*Klein et al*., 1998]. Consequently, research efforts have focused on improving estimates of sub-canopy SCA in forests. The algorithm used for operational SCA products from MODIS employs the normalized difference vegetation index (NDVI) in addition to the NDSI as criteria for

detecting snow in forests [*Klein et al*., 1998]. The NDVI, which is a normalized ratio of R_{NIR} and reflectance in the visible red band (R_{RED}), tends to decrease when snow exists in forests because snow will increase the overall R_{VIS} with respect to R_{RED}. Therefore, when the NDVI is between about 0.1 and 0.5, the pixel can be mapped as snow, even if the NDSI is less than 0.4 [*Klein et al.*, 1998; *Hall and Riggs*, 2007].

A second approach for canopy adjustment has been used with the MODSCAG and TMSCAG *f*SCA products. This adjustment ($fSCA_{ADJ}$) uses the vegetation fraction (*f*VEG) to scale observed *f*SCA [*Molotch and Margulis*, 2008; *Raleigh, et al*., 2013; *Rittger* et al., 2013].

$$fSCA_{ADJ} = \frac{fSCA_{TM}}{1 - fVEG} \tag{3}$$

This approach assumes that the spatial variability of *f*SCA is similar in sub-canopy and open locations. *Raleigh et al*. [2013] quantified the error associated with this vegetation fraction approach applied to MODSCAG *f*SCA and indicated that snow cover continued to be misrepresented even after application of a canopy adjustment.

1.2.2. Snow-vegetation interactions

Empirical evidence has long shown that snow accumulation and ablation processes vary spatially and temporally in relation to forest cover. Canopy snow interception and moderation of the snowmelt energy balance by forest cover influence

snow depth, SWE, and snowmelt rates, subsequently causing variable patterns in SCA [*Metcalfe and Buttle*, 1998; *Link and Marks*, 1999*; Storck et al*., 2002; *Musselman et al.*, 2008; *Varhola et al*., 2010*; Ellis* et *al.*, 2011]. Maximum snow depth, SWE and snow ablation rates are often greater in forest canopy openings because canopy characteristics, such as canopy density, tree leaf area index (LAI), and gap size, dictate snow interception [*Metcalfe and Buttle*, 1998; *Pomeroy et al*., 2002; *Storck et al*., 2002; *Lopez-Moréno and Latron*, 2008; *Varhola et al*., 2010]. These canopy characteristics also influence the energy balance by attenuating incoming solar radiation contributing to enhanced longwave radiation [*Ellis et al*., 2011]

Other specific canopy characteristics have been linked to quantifiable differences in snow properties. For instance, tree height has been connected to significant relationships in peak SWE and maximum ablation rate, with large tree heights corresponding to lower SWE and decreased ablation rates compared to short trees [*Varhola et al*., 2010]. Tree crown radius also affects snow properties, with a notably larger decrease in snow depth around individual trees with a crown radius greater than 3 m compared to trees with crown radii smaller than 2 m [*Musselman et al.,* 2008]. These forest canopy characteristics governing snow-vegetation interactions are a key factor to consider when predicting sub-canopy snow cover. Relating snow cover differences to tree canopy structure will be a key first step in improving canopy adjustments for *f*SCA.

1.2.3. Remote sensing of forest canopy

Quantifying the forest stand characteristics that govern snow-vegetation relationships rely on time intensive field inventories involving manual and sometimes subjective measurements of tree and forest attributes. Also, the sampling strategy used to develop site average canopy characteristics results in a tradeoff between including a sufficient number of samples to adequately represent the forest properties and covering a large enough area to properly characterize the variability in an entire forest stand [*Elzinga et al*., 1998]. Without broadscale efforts it may be impossible to capture the landscape scale vegetation characteristics that would be needed in a canopy adjustment for moderate resolution snow cover products. Remote sensing presents the opportunity to characterize canopy structure metrics at various resolutions, from plot scale tree structure to landscape scale characteristics.

Leaf area index (LAI) is a traditional means of assessing biomass and forest properties [*Song*, 2013]. This metric, which gives a measure of the leaf area per corresponding unit of ground area, can be derived from remote sensing data using regression relationships with the NDVI [*Chen and Chilar.,* 1996]. However, LAI is a two-dimensional representation of three-dimensional canopy structure and does not consider the vertical dimension of the forest canopy. Additionally, it is well know that the presence of snow under the forest canopy affects the magnitude of the NDVI [*Klein et al*., 1998]. This makes it difficult to use this index to assess the LAI when snow cover is present. Subsequently, it is necessary to use a three-dimensional approach to properly depict the vegetation structure that may affect the distribution of snow cover. This study

derives three-dimensional canopy structure from terrestrial laser scanning (TLS) at one scale and simple geometric-optical models (SGM) at larger scales to move up in scale to larger areas.

TLS is a relatively new technique for providing three-dimensional measurements of natural surfaces [*Olsen et al*., 2011; *Pirotti et al*., 2012]. Terrestrial scanners emit laser pulses that are reflected back to the instrument by solid surfaces that they encounter. The distances to these surfaces are determined based on the time period between laser transmittance and subsequent detection by the scanner. Measured distances are used to construct a three-dimensional point cloud of laser returns that are linked to horizontal and vertical coordinates determined by the geographic position of the scanner [*Hilker et al*., 2010; *Olsen et al*., 2011; *Vaccari et al*., 2013].

TLS has recently been employed to characterize forest canopy structure with 5-10 cm measurement accuracy [*Pirotti et al.,* 2012]. Canopy metrics derived from TLS point cloud data have shown meaningful agreement with field measured values of tree height, crown radius, and other canopy structure characteristics [*Hopkinson et al*., 2004a; *Hilker et al*., 2010; *Pirotti et al*., 2012; *Seidel et al*., 2012; *Vaccari et al*., 2013]. *Hopkinson et al*. [2004a] objectively extracted tree heights from TLS in a mature pine forest with an average difference of 1.5 m from field measured heights. *Maas et al*. [2008] indicated similar measurement accuracy for tree heights in a mixed coniferous forest, with automated tree height detection resulting in a mean difference of 1.5 m from *in situ* measurements. These results indicate that automated extraction of canopy attributes may

eliminate some of the sample bias and subjective measurements inherent in manual field data collection and provide a more comprehensive depiction of plot scale forest canopy.

At the stand scale, canopy extent, tree height, and crown radius can be extracted from high resolution aerial photographs using an SGM [*Chopping*, 2011; *Chopping et al*., 2012]. The CANopy Analysis from Panchromatic Imagery (CANAPI) algorithm exploits the contrast between bright and shadowed image pixels to differentiate tree crowns from shadowed background. Individual crowns can then be measured to determine crown radius and tree density. Tree heights, adjusted to account for terrain slope and aspect, can subsequently be determined based on geometric relationships between solar elevation angle and measured tree shadow lengths [*Chopping*, 2011]. When compared to field measurements, this algorithm successfully identified tree crowns in a mixed-conifer, old-growth forest, with a coefficient of determination (R^2) of 0.92 for fractional crown cover and up to 0.94 for tree heights [*Chopping*, 2011]. CANAPI has since been used as a validation tool for satellite derived canopy structure [*Chopping et al*., 2012].

At a larger spatial scale, a similar SGM can be used with satellite multi-angular reflectance data from NASA's Multiangle Imaging SpectroRadiometer (MISR) instrument to yield landscape scale estimates of tree canopy characteristics. MISR has nine cameras that view the Earth at fixed angles in the fore and aft directions along its orbital path and at four spectral bands (blue, green, red, and near-infrared) [*Diner et al*., 1999]. The spatial resolution of the red band (used here) is 275 m. The MISR SGM exploits the multi-angular pattern of reflectance from a forest canopy to determine

canopy structure and has been successfully used to map forest density and forest height in the Colorado Rocky Mountains [*Chopping et al*., 2009].

In the MISR SGM, atmospherically corrected multi-angular surface reflectance data are divided into a linear combination of illuminated or shaded background or tree crown components. The above-canopy reflectance is a function of crown structure and analysis yields estimates of average crown height, average crown radius, and average tree density for each 275 m image pixel [*Chopping et al*., 2009]. While the algorithm is automated, a user defined value for the contribution of background reflectance is required for optimal canopy separation. *Chopping et al.* [2009] established significant relationships between the MISR derived tree heights and vegetation heights retrieved by airborne LiDAR. As a result, landscape scale tree heights in the Colorado Rocky Mountains were effectively mapped with an average error of 2 to 5 m. Even over this rugged mountain landscape, the model achieved good agreement with metrics from LiDAR and aerial images [*Chopping et al*., 2009]. The ability to effectively map forest structure metrics at various scales will provide a link to snow processes moderated by vegetation, and can therefore, serve as a parameter for snow products at various resolutions.

1.3. Description of the study area

The central Oregon Cascades is a region where an accurate canopy adjustment is crucial since 85% of the snow zone has at least 20% forest canopy cover [*Coons*, unpublished]. This region receives 80% of its annual precipitation during winter months

and at high elevations the majority of this precipitation occurs as snow [*Tague and Grant*, 2004]. Twelve study sites were selected in this ecoregion to represent six elevations from 1100 to 1550 m in open and forested conditions. Ten of these sites are situated in the McKenzie River Watershed, while the other two are in the Middle Fork Willamette Watershed (Figure 1a). At five of the elevations, study sites were paired to include an open or low-density (LD) forest adjacent to a high-density (HD) forest. In the remainder of this paper, each site will be referred to by a unique identifier based its elevation and forest density category (Table 1). These sites all exhibit low relief, with a maximum average slope of 20 degrees.

The lowest elevation sites pass through portions of the Smith River and Kink Creek watersheds, sub-basins of the McKenzie River watershed, and incorporate a mosaic of timber clear cuts (Figure 1c). The high-density site (1100_HD) is composed of a mixed forest of Douglas-fir (*Pseudotsuga menziesii*), western hemlock (*Tsuga heterophylla*), and grand fir (*Abies grandis*). The trees are mature, dense, and evenly distributed. The adjacent low-density site (1100_LD) is in an open meadow composed of interspersed patches of smaller grand fir and noble fir (*Abies procera*).

The paired 1200 m elevation sites reside in the Middle Salt Creek Reservoir, a sub-basin of the Middle Fork Willamette watershed (Figure 1d). The sites consist of a Douglas-fir dominated forest stand (1200_HD) and an area that experienced a stand replacing burn in the early 1990's (1200_LD). The majority of the trees in 1200_HD are mature and continuous, however small proportion are of a younger cohort exhibiting

evidence of historical timber harvest. The 1200_LD site does contain a few smaller Douglas fir and many regenerating red alder (*Alnus rubra*).

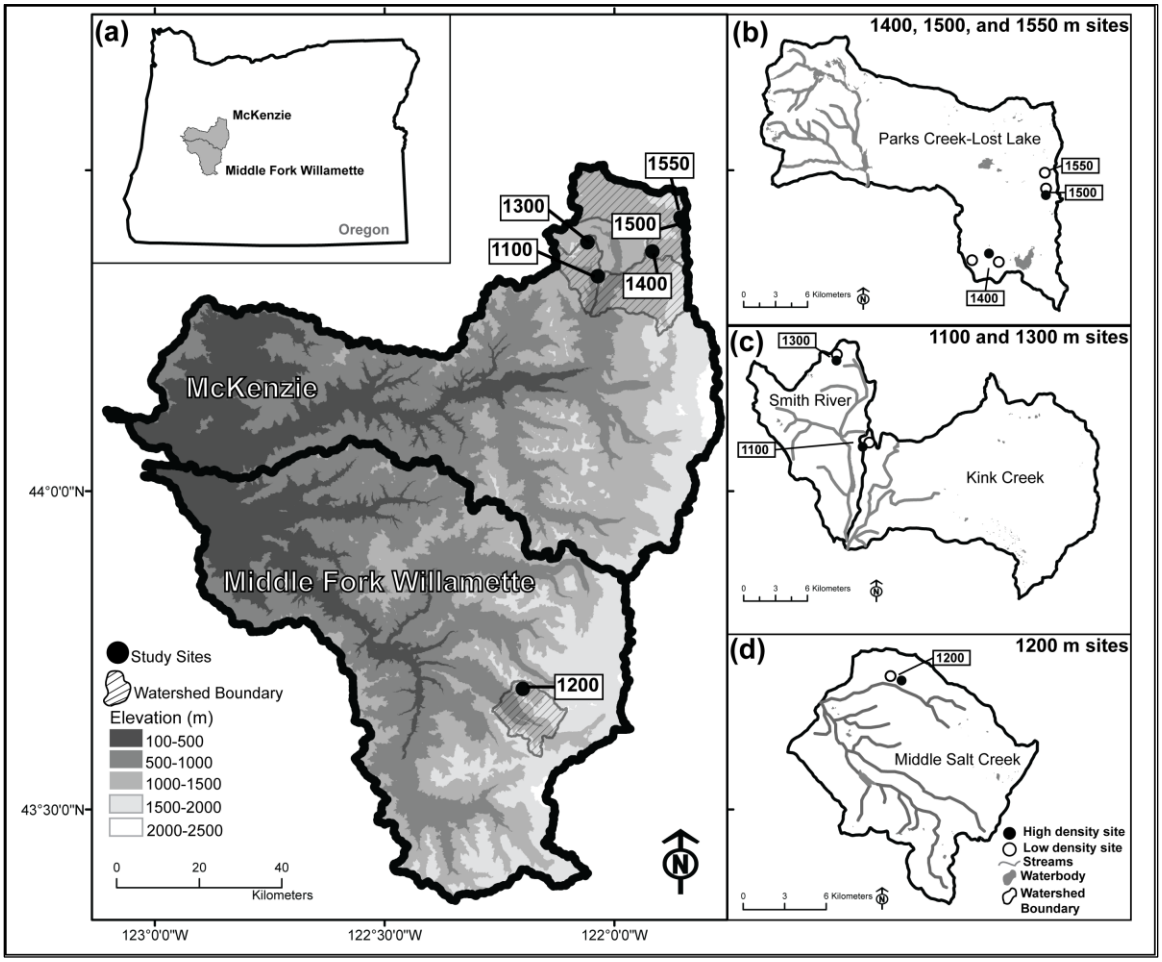

Figure 1. Locations of the 12 study sites in the McKenzie and Middle Fork Willamette watersheds within Oregon (a). The locations of paired high density (HD) and low density (LD) sites within the indicated sub-basins for 1400 m, 1500 m, and 1550 m sites (b); 1100 m and 1300 m sites (c); and 1200 m sites (d).

The study sites at the 1300 m elevation are directly north of the 1100 m sites in the Smith River watershed (Figure 1c). The 1300 m high-density site (1300_HD) has a continuous canopy of mature Douglas fir, western hemlock, and grand fir. The low-

density site (1300_LD) is a former clear cut. Regeneration of young noble and Douglas fir provide a sparse canopy.

Table 1. Characteristics of the 12 study sites

Site ID	Elevation (m)	Slope (degrees)	Aspect	Description
1100_LD	1110	5.8	Southeast	Open meadow
1100_HD	1130	9.7	East	High density tree canopy
1200_LD	1200	12.6	Southwest	Burned forest
1200_HD	1200	10.5	Southwest	High density tree canopy
1300_LD	1320	9.4	Northeast	Decade-old clear cut
1300_HD	1330	19.4	South	High density tree canopy
1400_LD	1400	2.2	Southeast	Low density tree canopy
1400_HD	1400	4.2	Northwest	High density tree canopy
1400_BU	1400	3.5	Southeast	Burned forest, no canopy
1500_LD	1470	1.9	Southwest	Burned forest, no canopy
1500_HD	1470	1.9	Northwest	High density tree canopy
1550_LD	1530	9.5	South	Burned forest, no canopy

The 1400 m, 1500 m, and 1550 m sites are all situated on the plateau of the high Cascades in the Parks Creek-Lost Lake watershed, which forms the headwaters of the McKenzie River Watershed (Figure 1b). The high-density site at 1400 m (1400_HD) is composed almost entirely of lodgepole pine (*Pinus contorta*). The trees are continuous with few forest openings, but many of the older trees at this site have succumbed to insect infestation and have begun to experience at least some needle loss. The paired low-density site (1400_LD) is an open forest predominately populated by mountain hemlock (*Tsuga mertensiana*), subalpine fir (*Abies lasioscarpa*), and lodgepole pine. The stand is characterized by patches of tree communities separated by large open areas. A third site at this elevation (1400_BU) falls within the perimeter of a wildfire that occurred in September 2011. The included area experienced a high severity burn and the only remaining standing trees are large with no living crown.

The 1500 m and 1550 m sites are separated by approximately 1 km and are near Santiam Pass, which marks the transition to the east side of the Cascades (Figure 1b). The 1500 m high-density site (1500_HD) has a fairly continuous forest canopy composed of mountain hemlock and lodgepole pine. The low-density site at 1500 m (1500_LD) falls within an approximately 10-year old stand replacing fire. The few remaining standing trees are dead with no living crown. Only one low-density site was included at the 1550 m elevation (1550_LD). This site is directly north of the 1500 m sites and includes the same high severity burn. The only standing trees present are dead with no canopy.

Chapter 2. Methods

2.1. General approach

To address the research questions presented in this study, several discrete analyses were carried out to examine patterns in satellite *f*SCA, *in situ* snow cover, and forest canopy structure. First, original satellite-derived *f*SCA and canopy adjusted *f*SCA ($fSCA_{ADJ}$) were both compared against ground-based observations of snow cover to assess the vegetation fraction canopy adjustment. The spatial and temporal accuracy of $fSCA_{ADJ}$ was then assessed across multiple study sites and errors were evaluated by comparing spatial and temporal patterns in forested and open sites. Errors in $fSCA_{ADJ}$ were further analyzed in comparisons with measured forest canopy characteristics. These same measured forest canopy characteristics were then related to estimates from TLS, high resolution aerial imagery, and multi-angular satellite reflectance data.

2.2. Snow observations

The distribution of snow cover across 11 of the 12 study sites was determined from *in situ* observations of snow cover from February to June 2012. The12th site, 1400_BU, was not included in the analysis of the $fSCA_{ADJ}$ and is only included to assess remote sensing techniques for characterizing vegetation structure. At the 1100 m, 1200 m, 1300 m, 1500 m, and 1550 m sites, the presence or absence of snow were derived from snow depth measurements at 5-m intervals taken along a single 500 m to 1000 m long snow course. These transects resulted in at least 50 sample locations for each site. A different sampling scheme was implemented at 1400_HD and 1400_LD, and is

described later. A sample location was considered snow covered if measured snow depth exceeded 1 cm. Snow surveys at each site occurred every 15 to 30 days along the same transect line, but slightly offset to avoid previously sampled locations.

To subsequently compare with satellite *f*SCA, the ground observations were spatially aggregated to the 30-m resolution of a Landsat 7 ETM+ pixel. The ground-based fractional snow-covered area ($fSCA_{GROUND}$) was then estimated by dividing the number of locations with observed snow cover (M_{Snow}) by the total number of observation locations (N):

$$fSCA_{GROUND} = \frac{M_{SNOW}}{N} \tag{4}$$

More intensive sampling was performed at the two 1400 m sites. At these sites snow presence/absence was recorded at 5-m intervals along 5 parallel transects through each site. The survey transects extended 100 m and were horizontally offset by 10 m, yielding a total of 100 observations per site. To investigate the temporal and spatial variability of snow cover at point locations, snow presence/absence was monitored at the same sample locations for a total of eight surveys occurring between 15 April and 20 June 2012. Each sample location was marked with flagging and recorded with a global positioning system (GPS) to ensure that the same position was monitored on each visit. The $fSCA_{GROUND}$ was determined in the same manner as described for the other sites (Eq. 4).

To provide another measure of $fSCA_{GROUND}$ and to capture snow cover patterns between field survey dates, Maxim iButton™ miniature temperature sensors were

deployed at all of the study sites. When buried under a few centimeters of soil, these temperatures sensors can indicate whether a location has snow cover based on the recorded diurnal temperature signal [*Lundquist and Lott*, 2008]. Snow cover has insulating properties that mute diel temperature fluctuations. Once snow has disappeared over the buried sensor, an obvious change occurs in the temperature data as the diurnal temperature pattern returns [*Lundquist and Lott*, 2008]. Nine temperature sensors were distributed systematically at the midpoint of each snow survey transect to overlap several adjacent Landsat ETM+ pixels. Using Eq. 4, based on the number of snow-covered sensors, the iButton fSCA ($f\mathrm{SCA}_{\mathrm{IB}}$) could be determined for any given date.

2.3. Forest inventory

In the snow-free season, characteristics of the forest canopy at each site were quantified in a conventional forest inventory. Sample locations were selected at 500 m intervals along the snow survey transects at the 1100 m, 1200 m, 1300 m, 1500 m, and 1550 m study sites, while at the 1400 m sites, sample locations occurred at the same 5 m intervals to coincide with the snow observations. At sample location in each site, the point-centered quarter plotless method [*Elzinga et al*., 1998] was used to estimate tree density. This method uses a small number of trees at sample locations and the distances between these trees to establish tree density. At each sample location, four quadrats were established aligned with the cardinal directions. The distance to the nearest tree in each quadrat was measured and stand tree density quantified Equation 5:

$$D = \frac{A}{\bar{d}^2} \quad (5)$$

Where D is tree density (trees per ha or 10000 m^2), A is the specified area (10000 m^2), and $\bar{d}$ is the average of the distances to the nearest tree (m) in the four quadrats at each sample location [*Elzinga et al*., 1998].

Tree height, tree diameter, crown radius, and species were also noted for the four closest trees at each sample location. The height was determined by finding the difference between the top of crown and base of tree inclination angles measured with a clinometer at a distance of 30 m from each tree. Tree diameter was measured on the uphill side of each tree at a height of 1.4 m from the forest floor and crown radius was determined as the distance from the tree bole to furthest extending branches comprising the crown area.

The forest canopy at each site was further characterized using skyward looking hemispherical photographs. The hemispherical photographs were captured with a Nikon Coolpix 990 digital camera equipped with a FC-E8 fisheye converter, which has a 180 ° field of view *[Inoue et al*., 2004]. Photographs were oriented north and taken at height of a 1 m above the ground surface. The hemispherical photographs were later assessed with Gap Light Analyzer 2.0 (GLA 2.0) to give a measure of the fraction canopy closure (CC) [*Frazer et al*., 1999]. This process involves converting each photograph to a binary image of tree canopy and sky. GLA 2.0 then determines the sky view fraction of each image and CC is assumed to be the complement.

The resulting CC were used to differentiate between open and sub-canopy locations at 1400_LD and 1400_HD. Based on visual inspection of the hemispherical photographs and field observations, sample locations were classified into low and high CC classes. The low CC class corresponds to CC < 0.65 and were assumed to represent open location where more snow cover would be detectable by TMSCAG. The high CC class includes locations with CC > 0.65, approximating areas where little snow cover would be detectable. To test the relationship between snow cover in open and sub-canopy locations, $fSCA_{GROUND}$ for high and low canopy classes was compared at 1400_LD and 1400_HD.

2.4. Satellite fractional snow-covered area

Cloud-free Landsat 7 ETM+ images were acquired from the United States Geological Survey [glovis.usgs.gov, accessed October 28, 2012] that coincided with the *in situ* snow observations. Landsat 7 provides reflectance data in 6 spectral bands at a 30 m spatial resolution. The return interval of the satellite is 16 days [landsathandbook.gsfc.nasa.gov, accessed January, 2013]. In 2003 the ETM+ scan line corrector (SLC) on Landsat 7 failed, resulting in swaths of missing data that vary in location depending on orbit. The "SLC-off" scenes still have about 78% data coverage [landsathandbook.gsfc.nasa.gov, accessed January, 2013], therefore Landsat 7 data could be used to provide reflectance data for the majority of the sites used in this study. Fractional snow-covered area was computed using the TMSCAG algorithm ($fSCA_{TM}$) [*Rittger et al*., 2013]. The vegetation fraction canopy adjustment of *Molotch and*

Margulis [2008] was then applied using the TMSCAG derived vegetation fraction (fVEG) to scale $f\text{SCA}_{\text{TM}}$ (Eq. 3) [*Rittger et al*., 2013].

Values of $f\text{SCA}_{\text{TM}}$ and $f\text{SCA}_{\text{ADJ}}$ for pixels overlapping the *in situ* snow surveys were extracted and compared to $f\text{SCA}_{\text{GROUND}}$ for surveys as close as possible to the satellite overpass date. When the overpass date did not coincide with the survey date, snow water equivalent (SWE) data from four nearby SNOTEL stations (Table 2) was consulted to assess any significant changes to $f\text{SCA}_{\text{GROUND}}$ that may have occurred during the interim period.

Table 2. The SNOTEL stations nearest to the study sites[a]

Site Elevation ID	SNOTEL Station	Station Elevation (m)	Distance to Station (km)
1100	Jump Off Joe	1070	12
1200	Salt Creek Falls	1070	9.5
1300	Bear Grass	1430	6.5
1400	Hogg Pass	1460	7
1500	Hogg Pass	1460	0
1550	Hogg Pass	1460	1.5

[a]Study sites are listed by the elevation of the paired sites that is used to identify them in this analysis.

Errors in $f\text{SCA}_{\text{ADJ}}$ were determined as the difference from *in situ* measurements:

$$\text{Error} = fSCA_{ADJ} - fSCA_{GROUND} \tag{6}$$

Therefore, negative errors, or errors of omission, represent underestimates of snow cover, and positive errors, errors of commission, correspond to overestimates of snow cover. The average error for pixels falling within each study site was investigated based on site density classification, elevation. This error was also related to site averages of CC from

the hemispherical photographs and field measured tree height, crown radius, and tree density.

2.5. Remote sensing of forest canopy

In August 2012, TLS data were obtained for three sites at 1400_LD, 1400_HD, and 1400_BU. Although we did not measure snow cover at this site, the 1400_BU site was included in this analysis to test the ability of TLS to characterize the range of forest types present in the snow survey study sites. The scan areas each encompassed sample locations that were included in the forest inventory.

Data were collected using a Reigl VZ-400 laser scanner equipped with a Nikon D700 camera and Trimble R8 GNSS receiver. This instrument has a range up to 600 m and a reported measurement accuracy of 0.5 cm [*Reigl*, 2013]. The scanner was positioned in a circular pattern at six evenly spaced positions, separated by about 20 m. Initial processing of TLS data was completed using Reigl RiScan Pro and Maptek I-Site Studio software. This pre-processing included optimization of yaw angles (rotation of the scanner in the vertical direction) and co-registration of point clouds from the separate scans based on GPS data, reflective markers deployed during data collection, and the internal inclination sensors on the scanner [*Olsen et al.,* 2011]. The remainder of the TLS data processing was carried out using ESRI ArcMap 10.1 software.

In ArcMap, the co-registered point clouds for each of the three study sites were converted to 0.1 m grids representing the maximum and minimum elevation returned over each grid cell. The resulting grids were cropped to include only areas of the highest

density point returns and exclude spurious data. After filling data gaps, the minimum grid, assumed to represent the bare ground surface, was subtracted from the maximum grid representing the tree canopy. This resulted in a surface representing the elevation of the tree canopy.

The spatial analyst tool in ArcMap was used to determine the crown radius and tree height of individual trees. For this method, the tree height elevations were inverted and individual tree canopies were treated as discrete "watersheds", similar to the approach described by *Koch et al.* [2006]. The local low point in the inverted grid, corresponding to the maximum height for each tree, was determined and the watershed tool was then used to delineate the canopy extent for each tree peak. Subsequently, the geometry of the resulting "watersheds" was determined to yield the crown radius. The zonal maximum within each tree crown was determined as the tree height. Some manual editing was still required to remove erroneous canopies and to separate tightly clumped trees into discrete elements. Overall however, this technique proved satisfactory for delineating and measuring individual trees from the TLS data.

Aerial digital photographs from the National Agriculture Imagery Program (NAIP) were acquired for the summer of 2011 to cover the extent of 9 of the 12 study sites. The 1500_HD and 1500_LD sites were not included in the vegetation remote sensing analysis. NAIP images include red, green, and blue bands, have a spatial resolution of 1 m and are orthorectified yielding a horizontal accuracy of 6 m [*USDA*, 2009]. Tree height, canopy radius, and tree density were extracted using the CANAPI algorithm [*Chopping*, 2011]. The algorithm was constrained using field measured values

of crown radius and tree density and was adjusted to account for site slope and aspect. The CANAPI processing window for each NAIP image was restricted to 112 m^2 centered on the midpoint of each snow survey transect. The images for the 1400 m sites also coincided with the three plots used in the TLS canopy analysis.

Data from MISR pixels covering the same extent as the NAIP images in the CANAPI analysis were analyzed using the SGM described by *Chopping et al*. [2009]. MISR images from numerous satellite overpasses during the summers of 2011 and 2012 were obtained to ensure complete data coverage and account for changes to canopy structure that resulted from the fire at 1400_BU during September 2011. The results from the SGM for the pixel covering the extent of each snow survey were used to characterize the site forest canopy. If the site was covered by multiple MISR pixels, the average value computed from those pixels was used to determine the site canopy structure metrics.

Tree height, crown radius, and tree density values that were extracted from each of these techniques to give a site average for each metric. These averages were compared to the averages from field measured values for each site. The overall ability of each method to depict canopy characteristics, along with the possibility of a scaling relationship, was assessed by plotting the remote sensing derived metrics against the field measured values.

Chapter 3. Results

3.1. Comparison of satellite *f*SCA to ground snow cover

According to reports from the National Resources Conservation Service [*NRCS*, 2013], the total basin snow water equivalent in 2012 was reported as 111% of the long-term average in the McKenzie River watershed and 107% of the long-term average in the Middle Fork Willamette Watershed. The winter was characterized by a dry period during February and March when little snow accumulation occurred and basin SNOTEL stations and snow courses reported SWE amounts about 50% of the long-term average. This deficit was augmented by higher than average precipitation in April-May and SWE amounts were above 100% of average at the end of April in both basins [*NRCS*, 2013].

Because of data recording issues and the loss of several sensors during spring snowmelt, a time series of snow cover could not be established from the miniature soil temperature sensors. However, the limited data from the 10 sensors that were recovered did reinforce the utility of soil temperature sensors for future analyses by clearly showing the temporal snow cover patterns over the sensors. For example, Figure 2 shows intermittent snow cover over a sensor at 1200_HD prior to mid-February. The sensor was then snow-covered until April 21, when the recorded temperature data again showed a diurnal signal. Field surveys in mid April confirm that there were soil patches present at this site. Yet, since a complete record of data could not be obtained for all of the sensors, the temperature sensors were not included in the remainder of the analysis.

There were limited cloud free Landsat scenes that coincided with the 2012 field snow observations. Three dates were completely cloud free over the study basins that contain the field sites, 24 February, 14 May, and 15 June (Figure 3). Snow cover was

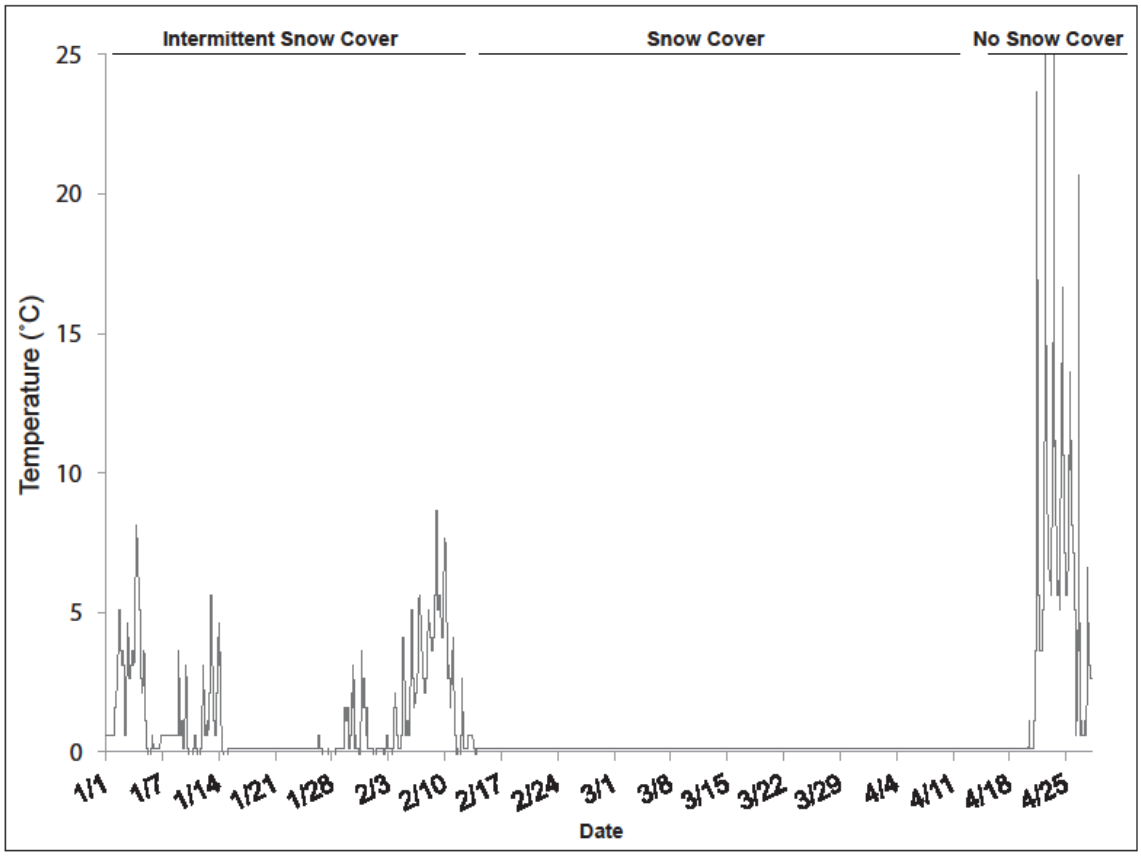

Figure 2. Temperature data for winter and spring 2012 from a buried soil temperature sensor in 1200_HD.

most extensive across the study basins for the 24 February overpass, while the study basins were only partially covered on 14 May. Snow cover was only present in the highest portion of the basins on 15 June.

A span of 7 to 13 days occurred between the February 24 Landsat overpass and the snow surveys. All of the SNOTEL stations recorded an increase in SWE during this time period (Figure 4). Therefore, it is possible that any bare ground present during the Landsat overpass would be covered for the field surveys, thereby resulting in an overestimate of $fSCA_{GROUND}$ by the satellite methods.

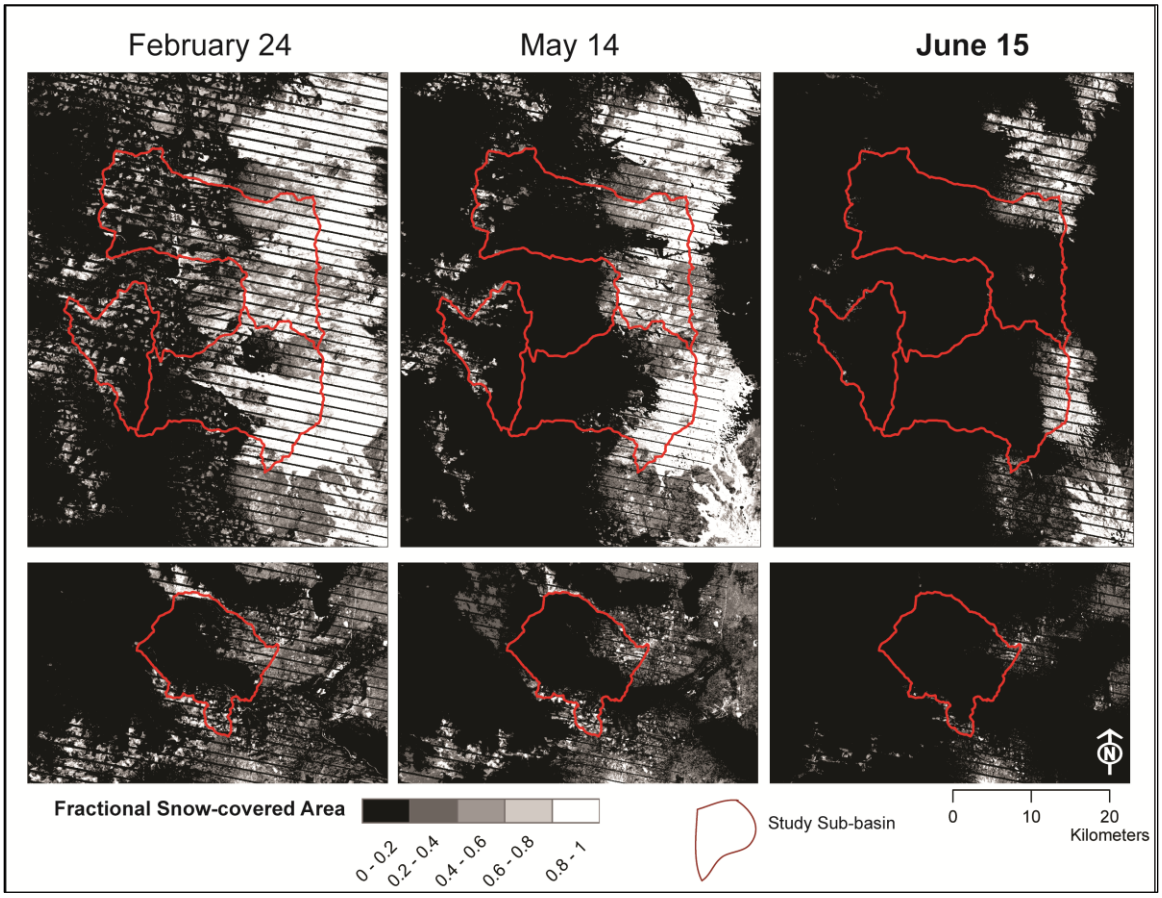

Figure 3. TMSCAG *f*SCA in the study basins for February 24, May 14, and June 15 2012.

Despite this possible source of error, the February 24 $fSCA_{TM}$ was included in the analysis because field surveys in early February indicate at least 90% snow cover at each site. During this period there was no decrease in recorded snow depth at nearby SNOTEL sites. Consequently, we assume that the area of bare ground present on the Landsat overpass date was likely minimal.

There was only a 1-day gap between the Landsat image acquisition on 14 May and the field surveys and we assume that changes in snow cover were insignificant. For the 15 June Landsat image, the field surveys at the 1400 m sites occurred 3 days prior to

and the 1500 m surveys occurred 2 days after the image acquisition date. The Bear Grass SNOTEL station reported a 24% loss in SWE from 12 June to 15 June and a 32% decrease from 15-17 June. The other SNOTEL stations were snow free by 12 June. It is possible that the *f*SCA during the interim period changed significantly, but the date was still included in the analysis.

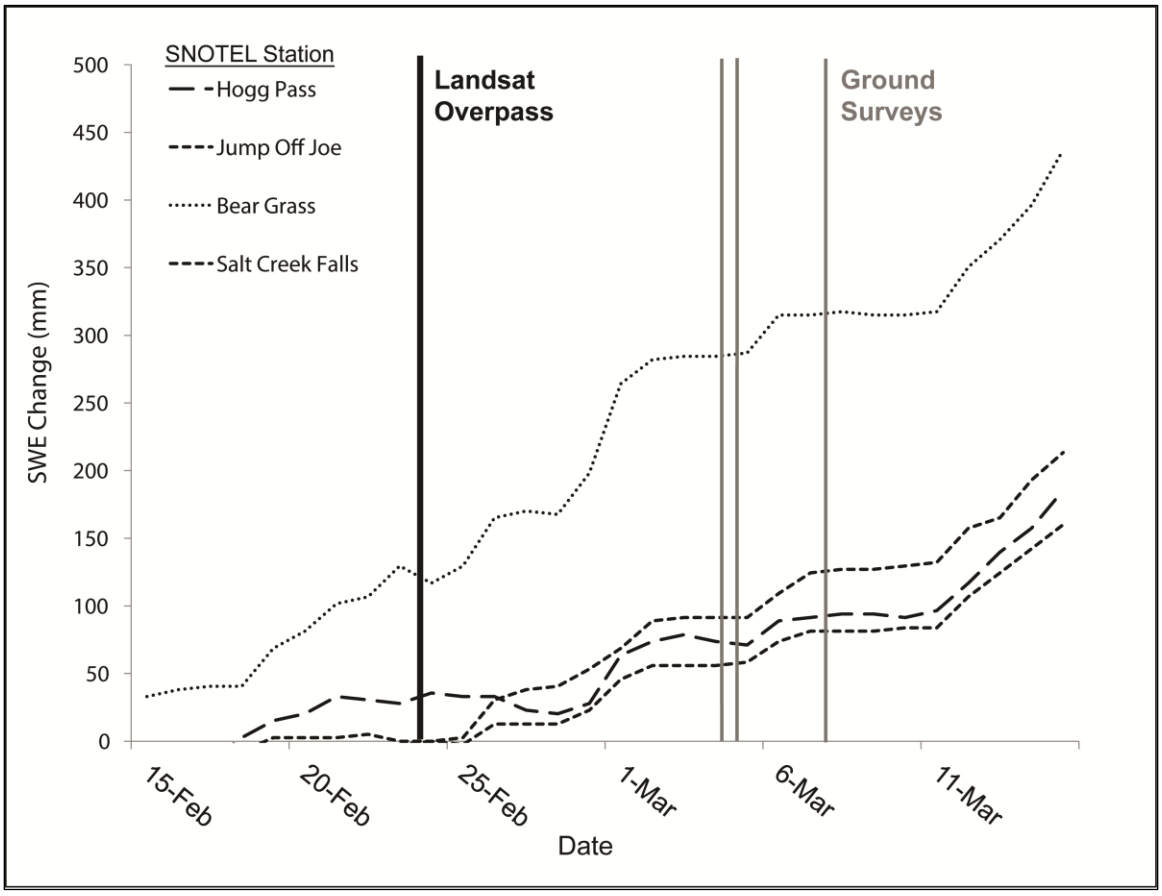

Figure 4. The recorded increase in SWE between the 24 February, 2012 satellite overpass and field surveys.

On 24 February ground surveys indicated the $fSCA_{GROUND}$ was close to 1 for all sites. Application of the vegetation fraction canopy adjustment resulted in substantial

improvement over $f\mathrm{SCA}_{\mathrm{TM}}$ when compared to total $f\mathrm{SCA}_{\mathrm{GROUND}}$ at 1100_LD, with the adjustment increasing the fSCA from 0.4 to 1.0 (Figure 5a).

At the 1100_HD site, the viewable gap fraction was too low for TMSCAG to detect any snow cover, so a canopy adjustment could not be applied. Both 1200 m sites fell in the SLS gap in satellite reflectance data, therefore these sites could not be included in the comparison. The adjustment resulted in some improvement over the $f\mathrm{SCA}_{\mathrm{TM}}$ for the 1300 m sites, but still failed to account for all snow cover, especially at 1300_HD where $f\mathrm{SCA}_{\mathrm{ADJ}}$ was still only 0.3 (Figure 5c). Estimates of $f\mathrm{SCA}_{\mathrm{GROUND}}$ were improved after the canopy adjustment was applied at both 1400 m sites and 1500_HD (Figure 5d-e). A canopy adjustment did not appear to be necessary for 1500_LD or 1550_LD as $f\mathrm{SCA}_{\mathrm{TM}}$ was comparable to $f\mathrm{SCA}_{\mathrm{GROUND}}$ (Fig. 5e-f).

By the time of the satellite overpass on 14 May, the 1100 m and 1200 m were completely snow free and unadjusted TMSCAG correctly identified no snow at these sites. At the 1300 m sites, $f\mathrm{SCA}_{\mathrm{ADJ}}$ was dramatically greater than $f\mathrm{SCA}_{\mathrm{GROUND}}$ for 1300_HD. The adjustment resulted in an estimate of 0.7 while the ground surveys reported close to zero snow cover (Figure 6a). The $f\mathrm{SCA}_{\mathrm{TM}}$ was more comparable to $f\mathrm{SCA}_{\mathrm{GROUND}}$ because minimal snow cover was only detected for one pixel, resulting in a site average fSCA of 0.03. The opposite pattern is observed at 1300_LD with $f\mathrm{SCA}_{\mathrm{TM}}$ failing to detect about 50% of $f\mathrm{SCA}_{\mathrm{GROUND}}$ and $f\mathrm{SCA}_{\mathrm{ADJ}}$ correctly identifying most snow cover.

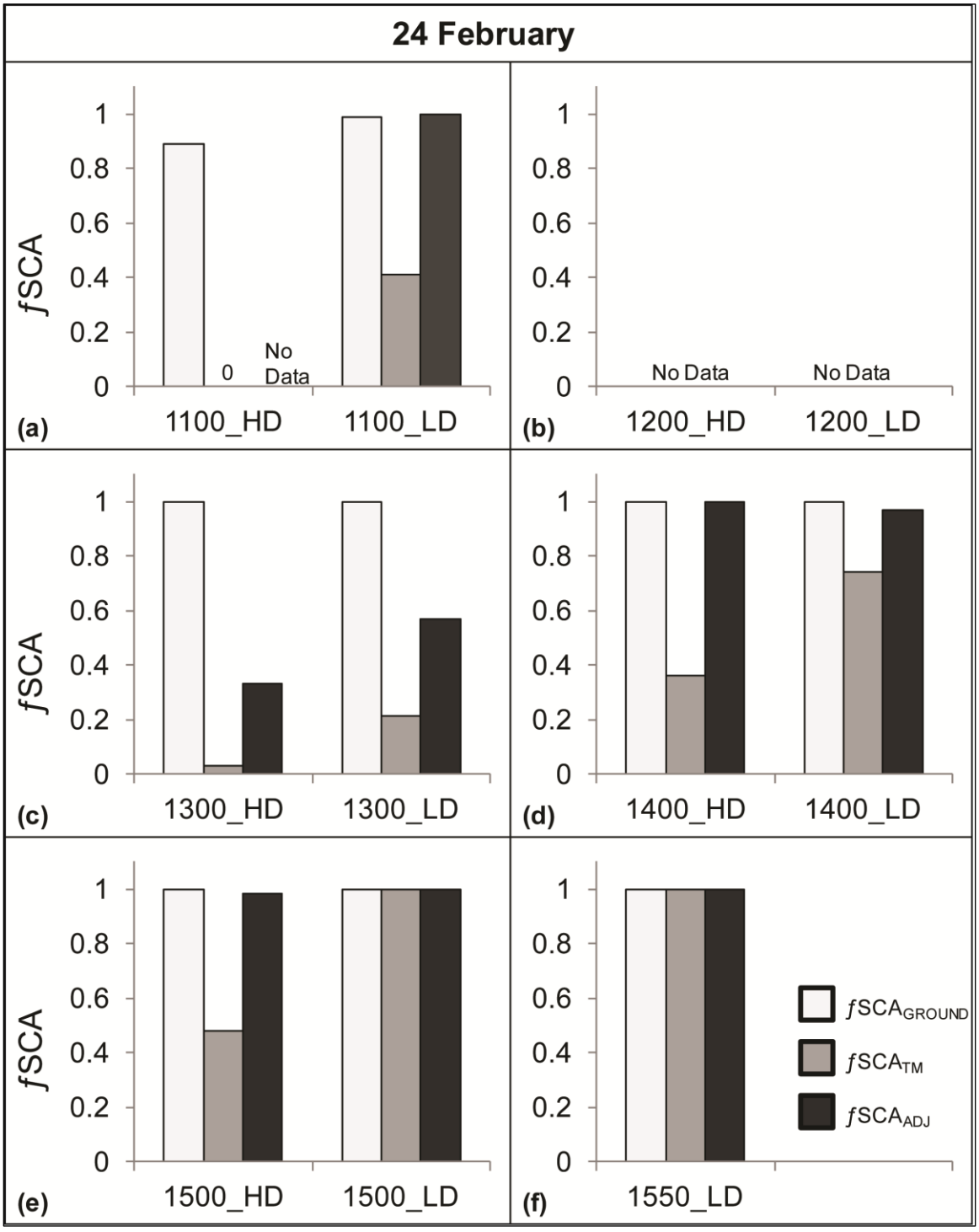

Figure 5. 24 February site average $fSCA_{TM}$, $fSCA_{ADJ}$, and $fSCA_{GROUND}$ for elevations represented by the paired sites at 1100 (a), 1200 (b), 1300 (c), 1400 (d), 1500 (e), and 1550 (f).

The 1400_HD site fell in a gap in reflectance data and could not be included. At the 1400_LD site, $f\text{SCA}_{\text{TM}}$ more closely approximated $f\text{SCA}_{\text{GROUND}}$, while $f\text{SCA}_{\text{ADJ}}$ overestimated $f\text{SCA}_{\text{GROUND}}$ by about 25% (Figure 6b). An adjustment may not have been necessary for 1500_LD because $f\text{SCA}_{\text{TM}}$ was within 8% $f\text{SCA}_{\text{GROUND}}$ (Figure 6c). However, at 1500_HD, the canopy adjustment resulted in considerably better representation of $f\text{SCA}_{\text{GROUND}}$ than $f\text{SCA}_{\text{TM}}$, which was only 0.4 despite ground surveys indicating complete snow cover. The $f\text{SCA}_{\text{TM}}$ was comparable to $f\text{SCA}_{\text{GROUND}}$ for 1550_LD (Figure 6d), indicating that an adjustment would not be necessary for this site, but the adjustment did not alter fSCA values by a considerable amount.

On 15 June, documented snow cover remained at only the 1400 m and 1500 m sites; 1550_LD was not surveyed. Despite there being snow cover within the detectable limit of TMSCAG for 1400_HD and 1500_HD, no snow was detected by the TMSCAG algorithm (Figure 7a, b). Therefore, a canopy adjustment could not be applied and up to 30% of snow cover was missed for these areas. The snow cover at the 1400 m sites may have actually been less at the time of the Landsat 7 overpass, as rapid melt may have occurred over the three days in the interim period after the ground surveys. Alternatively, at the 1500 m sites, $f\text{SCA}_{\text{GROUND}}$ may have been greater because the field surveys occurred two days after the satellite overpass.

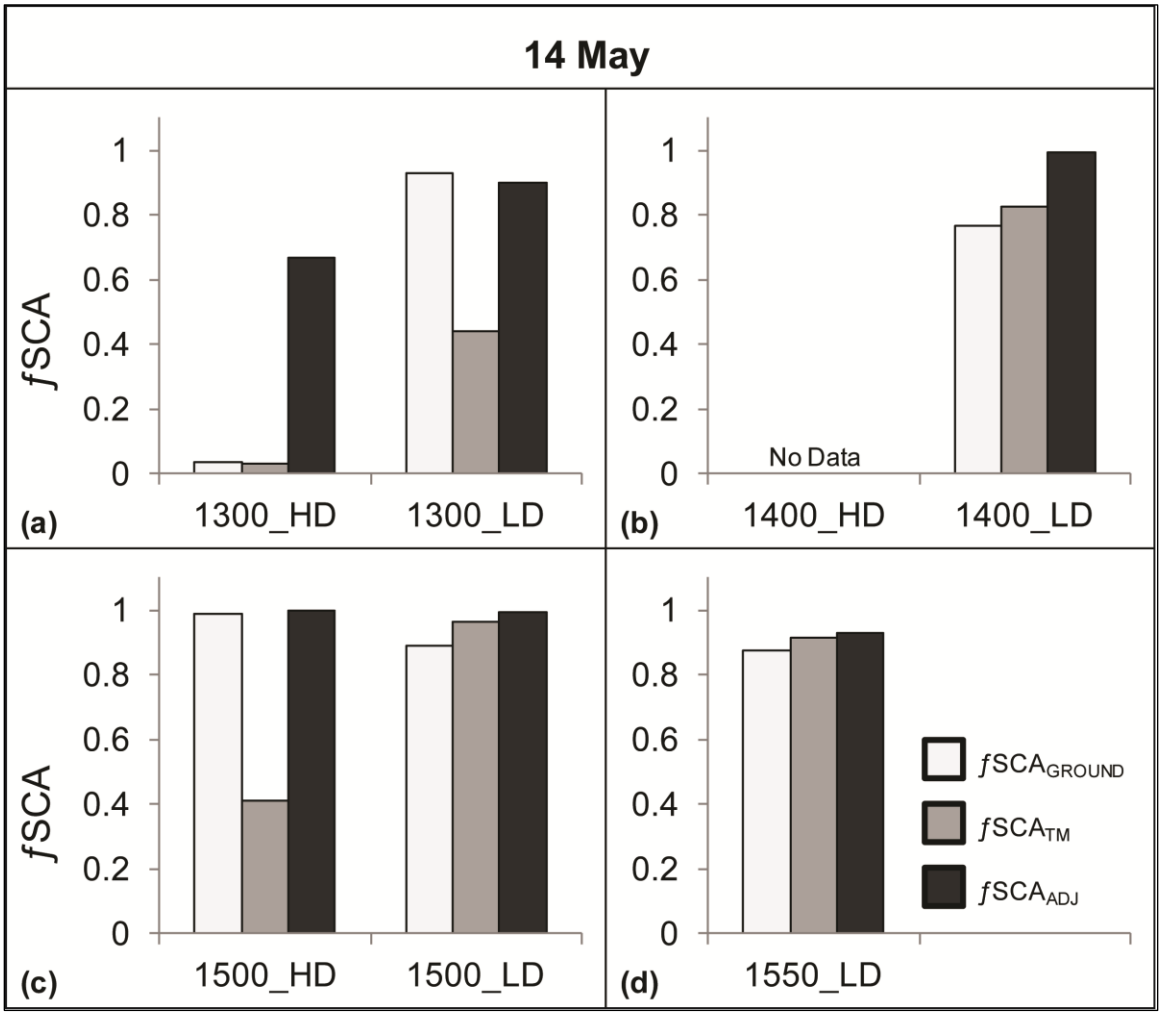

Figure 6. 14 May differences in $fSCA_{TM}$, $fSCA_{ADJ}$, and $fSCA_{GROUND}$ for elevations represented by the paired sites at 1300 m (a), 1400 m (b), 1500 m (c), and 1500 m (d).

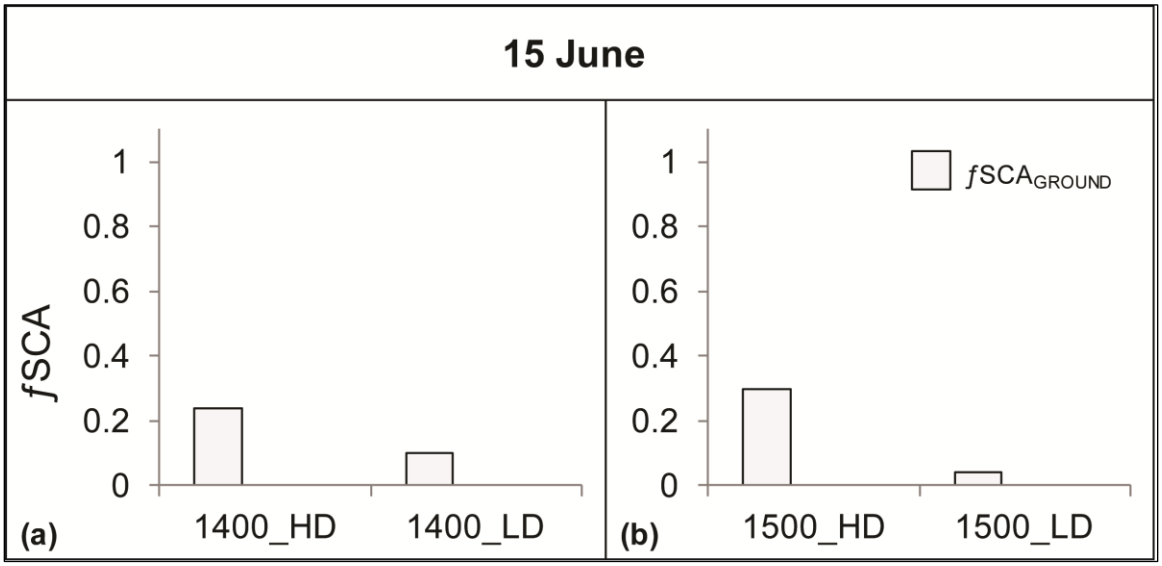

Figure 7. 15 June $f\text{SCA}_{\text{GROUND}}$ for elevations represented by the paired sites at 1400 m (a), and 1500 m. TMSCAG did not detect and fSCA for these sites.

3.2. Errors in canopy adjusted fractional snow-covered area

The comparison of $f\text{SCA}_{\text{TM}}$ and $f\text{SCA}_{\text{ADJ}}$ against $f\text{SCA}_{\text{GROUND}}$ indicate that the vegetation fraction adjustment improves fSCA estimates for some dates and locations, but improvements are not ubiquitous. Therefore, the error for $f\text{SCA}_{\text{ADJ}}$ (Eq. 6) is compared for the high and low-density sites across elevation and time. The two lowest elevation sites were excluded from analysis because of insufficient data. Only 1100_LD had data coverage for any of the dates (24 February) and the difference between $f\text{SCA}_{\text{ADJ}}$ and $f\text{SCA}_{\text{GROUND}}$ was close to zero for this date. Therefore, only sites with an elevation of 1300 m or greater were included in this error analysis.

Regardless of date or forest density classification, sites at the 1400 m, 1500 m, and 1550 m sites have lower error than the 1300 m sites suggesting that elevation may play a role in the snow patterns that affect error in $f\text{SCA}_{\text{ADJ}}$ (Figure 8). These results are

also suggestive of a temporal trend in the error. The magnitude of the error for the 1300_HD site remains approximately the same in magnitude between 24 February (-0.67) and 14 May (0.63), but the sign associated with the error changes from negative (error of omission) on 24 February to positive (error of commission) on 14 May. Conversely, the error for 1300_LD decreases with time, from an omission error of approximately 40% on 24 February to almost no error on 14 May.

For sites above 1300 m, errors of commission tend to occur in low-density forests regardless of elevation on 14 May, while errors of omission tend to occur in the high-density forests for all dates when an error was observed. The highest elevation site exhibits the lowest error of any of the sites regardless of date. However, the effectiveness of the canopy adjustment at 1400_HD and 1500_HD sites appears to decrease slightly with time because the magnitude of error increases between the February, May, and June dates. These elevational and temporal trends suggest that $fSCA_{ADJ}$ error increases with elevation as snowline recedes in the spring, but the error at high elevations is mostly restricted to high-density forests where errors of omission occur. There is also an apparent association between the forest density classification and the ability of the canopy adjustment to account for sub-canopy snow. At each elevation, the HD site tends to have errors that are equal or greater than the error for the LD site regardless of date. The 1500 m sites seem to be an exception because 1500_LD has a greater error (0.10) than 1500_HD (0.01) on 14 May.

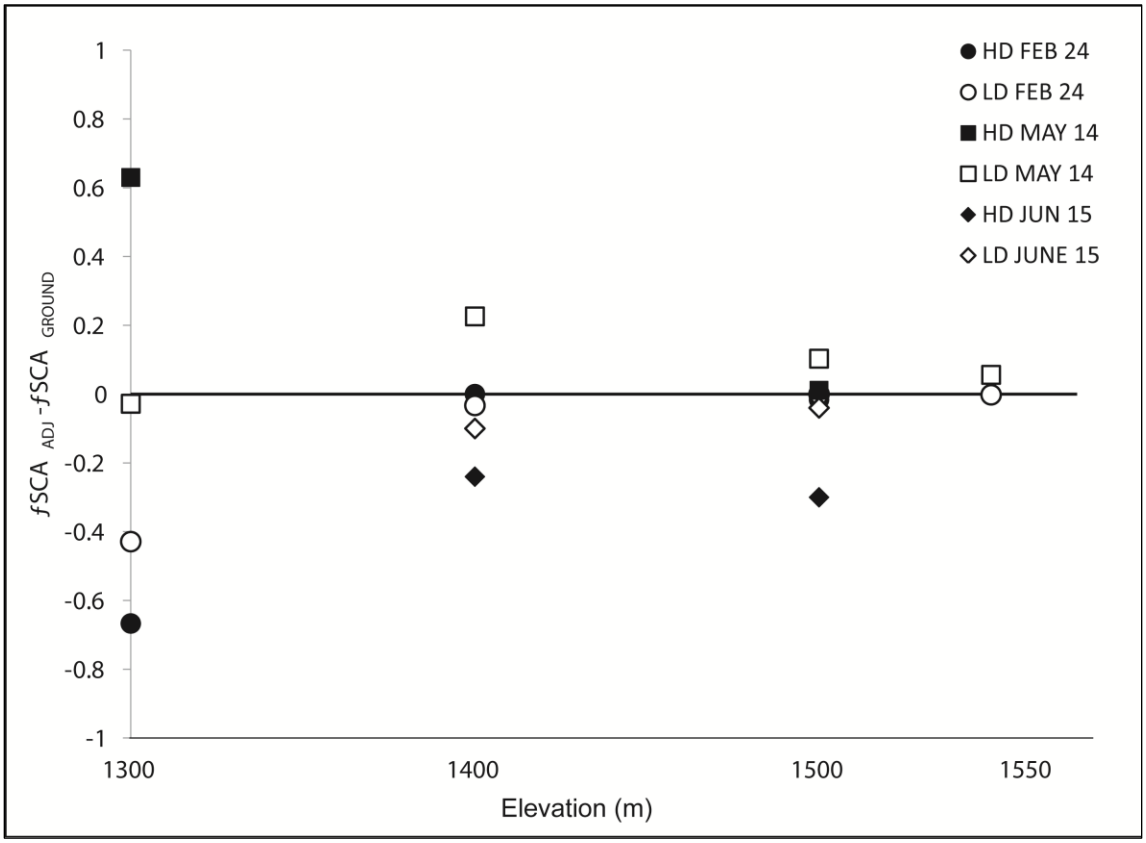

Figure 8. Difference between $f\text{SCA}_{\text{ADJ}}$ and $f\text{SCA}_{\text{GROUND}}$ for all HD and LD sites on 24 February, 14 May, and 15 June.

3.3. Asymmetries between snow in open and sub-canopy locations

The error analysis of $f\text{SCA}_{\text{ADJ}}$ suggests that errors of omission correspond to underestimates of $f\text{SCA}_{\text{GROUND}}$ where sub-canopy snow remains undetected. Errors of commission then correspond to overestimates where the sub-canopy snow fraction is less than the snow fraction in canopy gaps. To verify this assumption and subsequently examine variability in sub-canopy snow within sites at a single elevation, the snow fraction for open (SF_O) and sub-canopy (SF_{SC}) observation locations were compared within 1400_HD and 1400_LD. The open and sub-canopy locations were determined

based on the CC derived from hemispherical photographs taken at each that location. Different spatial and temporal patterns in SF_O and SF_{SC} were observed at each of these sites. To first test whether CC would serve as an effective proxy for the unobservable snow fraction in TMSCAG, CC was compared to *f*VEG (Figure 9). About 90% of the variation in *f*VEG could be explained by CC, verifying this premise. Therefore, observation locations with high CC can justifiably approximate sub-canopy locations having a greater potential to obscure sub-canopy snow.

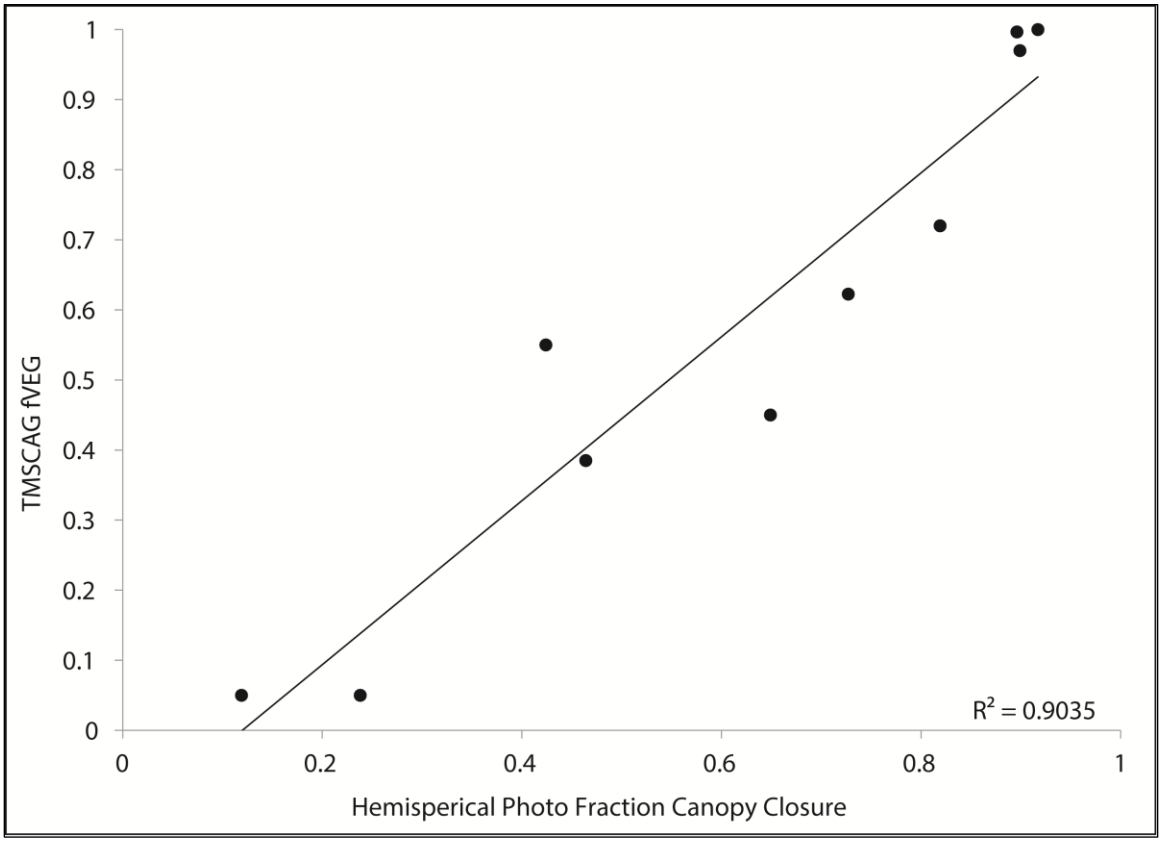

Figure 9. Relationship between canopy closure from hemispherical photos (CC) and fraction vegetation (*f*VEG) detected by TMSCAG, indicating that CC can serve as an effective proxy for the gap fraction observable by TMSCAG.

At 1400_LD, SF_{SC} and SF_O were comparable for the first three surveys, April 15, May 4, and May 13 (Figure 10a). Following these surveys, SF_O was considerably higher than SF_{SC}, with 53% of the open locations still observed to have snow cover and only 33% of the sub-canopy locations retaining snow cover. This trend continues with SF_O remaining greater than SF_{SC}, which corroborates positive errors in $fSCA_{ADJ}$ on 14 May at this site. The canopy adjustment was assuming snow under the canopy, when this snow was actually the first to disappear.

In contrast to 1400_LD, the SF_O and SF_{SC} at 1400_HD were similar for the majority of the survey period, but SF_{SC} was consistently greater than SF_O (Figure 10b). In mid to late June, as snow began to completely disappear, snow only remained in sub-canopy locations and SF_O became zero much earlier than $SF_{SC.}$ The timing of the surveys were unable to adequately capture the disappearance of the SF_O, however these results help to explain the inability of TMSCAG to detect snow at this site on 15 June, as the only snow remaining was in sub-canopy locations with the highest CC. When comparing the open and sub-canopy SF between 1400_HD and 1400_LD, it is apparent that both SF began to decrease more rapidly at 1400_LD with SF_{SC} decreasing much more quickly than either SF at 1400_HD.

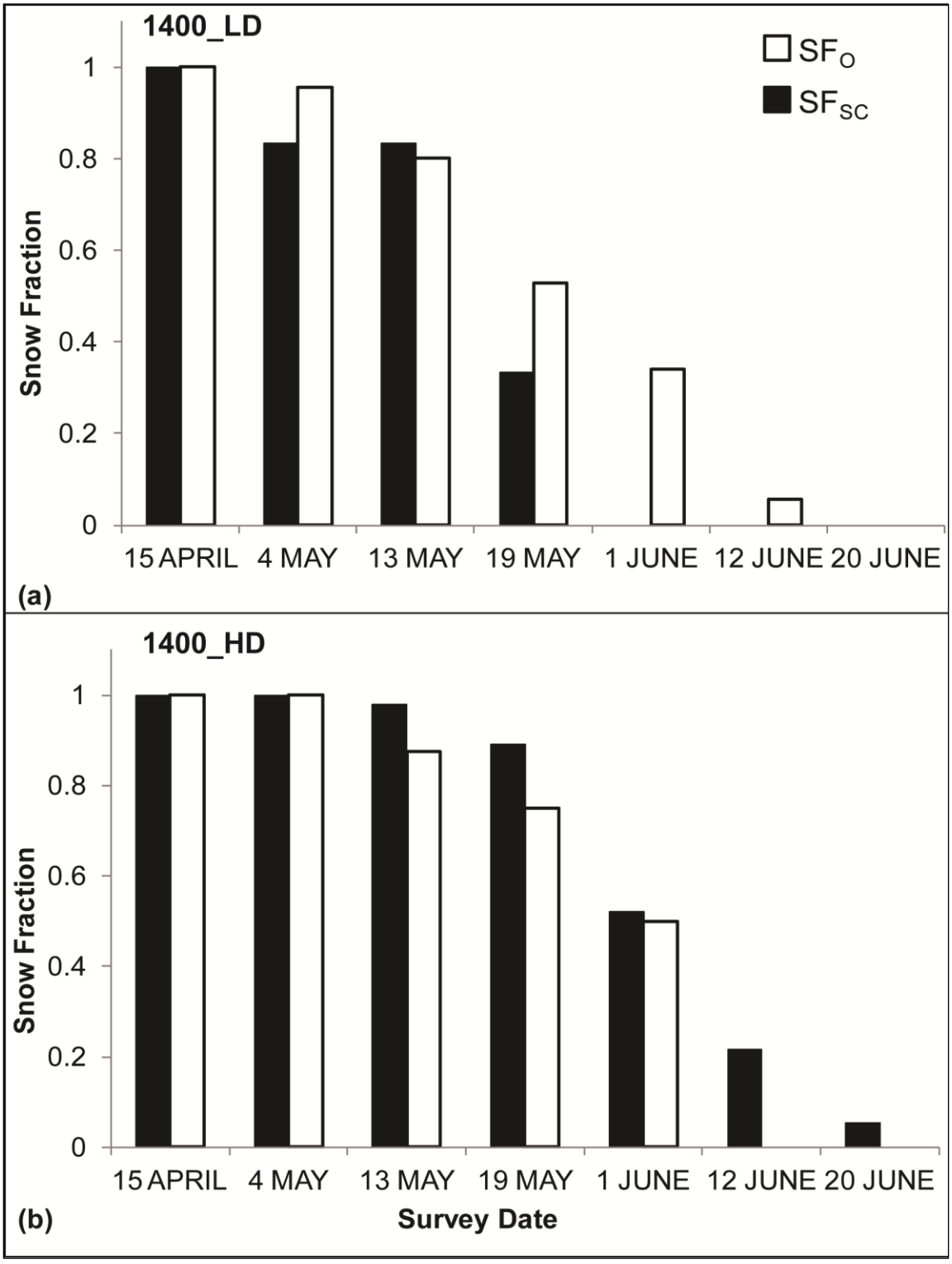

Figure 10. The snow fraction for open (SF_O) and sub-canopy (SF_{SB}) observation locations in 1400_LD and 1400_HD.

The comparison of SF_O and SF_{SC} was not repeated for the sites at other elevations. However, comparing the overall SF depletion for the paired high and low-density forests helps reveal if similar patterns may be observed at these other elevations. Depletion curves for the SF indicate that a longer duration of snow cover at the high-density forest, like for the 1400 m sites, is not pervasive across elevations (Figure 11a-d).

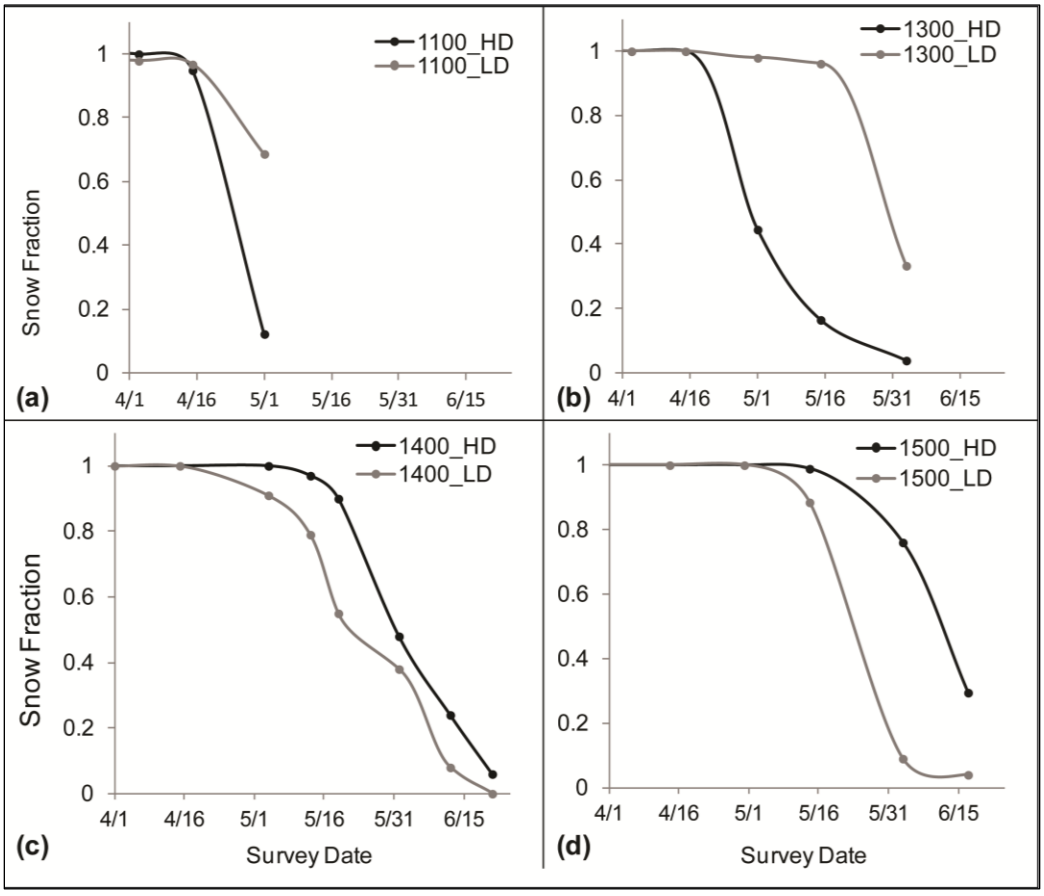

Figure 11. Depletion of the snow cover fraction for paired sites at 1100 m (a), 1300 m (b), 1400 m (c), and 1500 m elevations.

Snow persisted longer at 1100_LD and 1300_LD than at 1100_HD or 1300_HD (Figure 10a-b). Yet, the opposite pattern is observed for sites at 1400 m or above. Snow persisted longer at 1400_HD and 1500_HD compared to 1400_LD and 1500_LD (Figure 11c-d). Snow survey frequency was not high enough to capture these patterns at the 1200 m paired sites.

These results are in agreement with the differences observed between $fSCA_{ADJ}$ and $fSCA_{GROUND}$ at these sites. The $fSCA_{GROUND}$ was overestimated by almost 70% at 1300_HD on 14 May, when it is likely that snow at this site was melting under the large tree canopies and persisting in the larger canopy gaps. On 15 June, $fSCA_{GROUND}$ at 1500_HD went completely undetected by TMSCAG because similarly to the 1400_HD site, the only remaining snow was likely under high density canopy cover.

3.4. Forest structure and canopy adjustment error

The canopy structure at each of the study sites was quantified with forest inventory measurements, which revealed a wide range canopy attributes (Table 3). However, there was a lack of a strong relationship between the site-averaged canopy structure metrics of CC, tree height, canopy radius, and tree density and the average error associated with the vegetation fraction canopy adjustment (Figure 12 a-l). This may be attributable to the limited sample sizes for the 14 May and 15 June dates and limited representation of canopy characteristics across all elevations. The lack of significant trends make it impossible to form robust inferences on the bearing of these canopy

structure parameters on error in $fSCA_{ADJ}$, but the observed patterns do help provide perspective on how canopy structure may hinder this canopy adjustment's ability to account for snow. Hence, observed error in $fSCA_{ADJ}$ (Eq. 6) for the 24 February, 14 May, and 15 June satellite dates are addressed individually for each canopy structure metric (Figure 12 a-l). Due to lack of complete data coverage, the 1100 m and 1200 m sites were not included in this analysis. Based on the opposing snow depletion patterns revealed in Figure 10, the 1300 m sites are displayed differently than the 1400 m, 1500 m, and 1550 m sites in Figure 12.

Table 3. Mean and standard deviation (St. Dev.) of field measured canopy characteristics

	Tree height (m)		Crown radius (m)		Tree diameter (cm)			Canopy closure fraction (CC)	
Site ID	Mean	St. Dev.	Mean	St. Dev.	Mean	St. Dev.	Tree density (trees/ha)	Mean	St. Dev.
1100_LD	8.9	3.3	1.9	0.6	17.3	5.8	100	0.42	.29
1100_HD	33.7	18.8	4.7	1.7	52.1	33.3	330	0.90	.74
1200_LD	14.7	7.9	2.3	0.8	25.0	16.0	660	0.82	.13
1200_HD	26.3	3.0	3.6	0.4	37.3	6.9	1070	0.92	.02
1300_LD	11.8	3.9	2.0	0.5	19.0	4.2	190	0.56	.22
1300_HD	21.2	12.6	3.4	1.2	36.5	24.8	420	0.90	.02
1400_LD	9.2	4.7	1.2	0.6	22.0	10.1	550	0.46	.11
1400_HD	9.9	4.8	1.2	0.5	17.2	6.3	1800	0.73	.07
1400_BU	9.4	4.9	0.7	0.6	22.0	9.0	1400	0.22	.04
1500_LD	10.4	6.7	1.1	0.7	28.5	16.3	160	0.17	.13
1500_HD	14.5	6.9	1.3	0.4	20.8	8.3	1360	0.69	.09
1550_LD	12.8	6.2	1.4	0.8	30.6	13.2	270	0.24	.05

On 24 February, any $fSCA_{ADJ}$ errors are errors of omission for all sites, indicating that all inconsistencies resulted from underestimates in snow cover (Figure 8). It is difficult to determine if the error is a result of elevation controls or CC on this date. The

sites with the highest error are the two 1300 m sites (Figure 12a), and although 1300_HD has the highest CC (0.90), 1300_LD has a moderate CC (0.56).

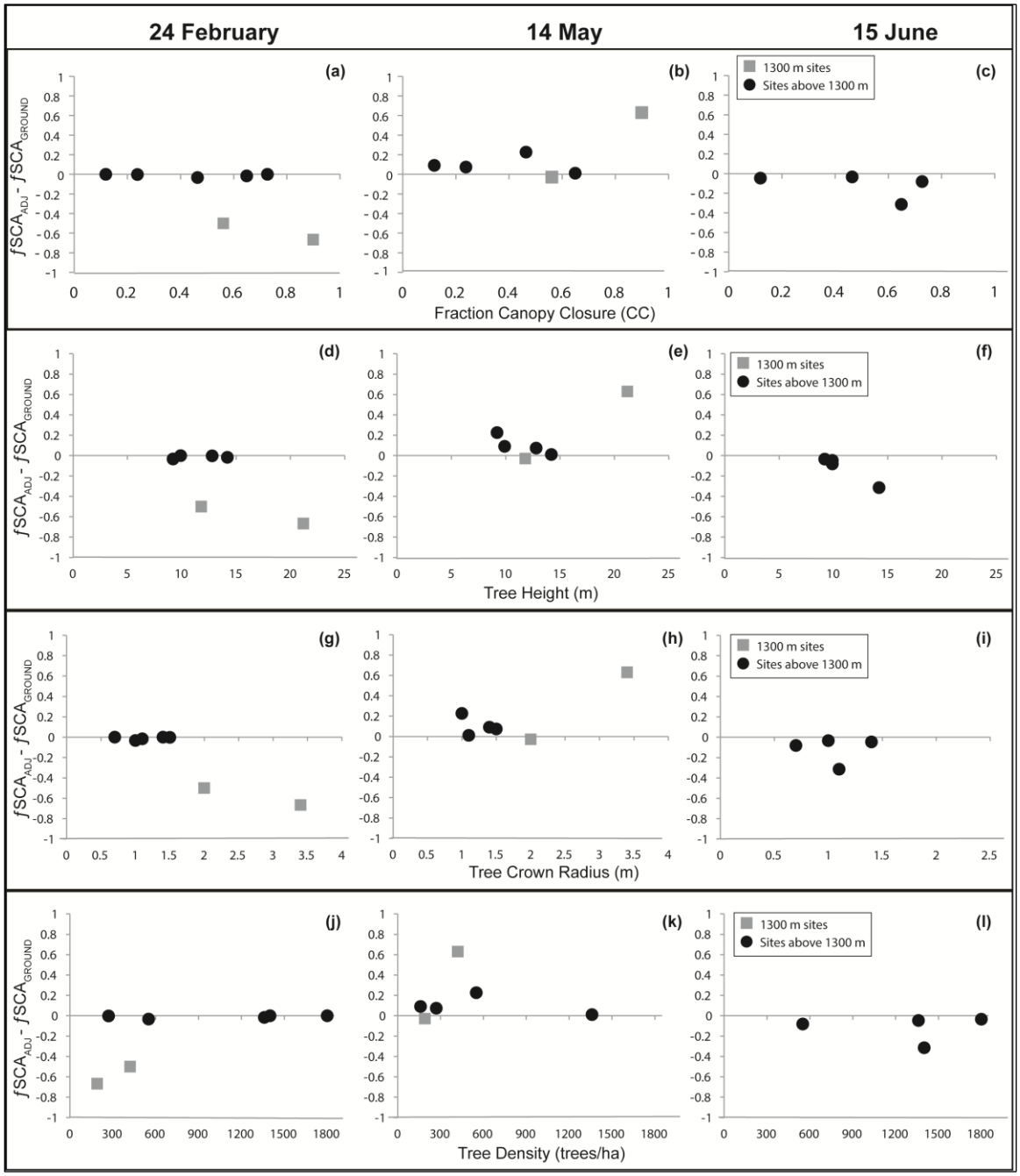

Figure 12. The error in $fSCA_{ADJ}$ compared to CC, tree height, tree crown radius, and tree density for the three Landsat data acquisition dates.

On 14 May, the error is highest for the site with the highest CC (1300_HD), but the site experiencing the next greatest error (1400_LD) only has a CC of 0.46 (Figure 12b). Both of these errors were errors of commission. On 15 June, all sites have fairly small error except for 1500_HD (error = -0.3), which has a fairly high CC (0.69), but not the greatest represented by the sites (Figure 12c). The error at 1400_HD was considerably lower yet this site has a slightly greater CC (0.73).

Tree height shows a similar pattern to error as CC for 24 February and 14 May. 1300_HD has average tree heights considerably greater than the other sites with a site average of 21.2 m, but 1300_LD has average tree heights in the middle of the range (Figure 12d). This reinforces that it is the elevation of these sites, not the average tree heights that is causing the higher error at these sites on 24 February. On 14 May, error is greatest for the site with the tallest trees (1300_HD) and the second greatest error occurs for the site with the smallest average tree heights (1400_LD) (Figure 12e). Tall trees may be responsible for the greater error at 1500_HD on 15 June, as this site has average heights almost 4 m greater than the 1400_HD site (Figure 12f). However, it is difficult to determine if taller trees are a greater contributing factor or if the error is related to the slightly higher elevation at the 1500_HD site.

The two 1300 m sites have greater average crown radii than the high elevation sites, which on 24 February makes it seem as if crown radius may be indicative of areas where $fSCA_{ADJ}$ does not correctly account for snow (Figure 12g). However, 1400_LD has the smallest crown radii (1.2 m) of the included study sites and this site has the

second greatest error on 14 May (Figure 12h). Also, on 15 June, the site with the greatest error (1500_HD) has only a slightly greater average crown radius (1.3m) (Figure 12i). These contrasting results suggest that large crowns may be related to a decreased gap fraction that prevents TMSCAG from detecting snow through canopy gaps on 24 February when snow was extensive, but for these sites, crown size is not the sole factor that indicates areas where $f\mathrm{SCA}_{\mathrm{ADJ}}$ is misrepresenting $f\mathrm{SCA}_{\mathrm{GROUND}}$.

Tree density alone does not appear to have a strong bearing on locations where $f\mathrm{SCA}_{\mathrm{ADJ}}$ is most likely to misrepresent $f\mathrm{SCA}_{\mathrm{GROUND}}$. The 1300 m sites have densities lower than most of the high-density sites, so the higher error on 24 February does not appear to be linked to tree density (Figure 12j). On 14 May, it does not seem to be a contributing factor because 1300_HD and 1400_LD (the sites with the greatest errors) have tree densities in the middle of the range (420 and 550 trees per ha respectively) (Figure 12k). In June, the remaining relatively high-density sites had fairly low errors of omission (Figure 12l). There was higher error at 1500_HD (1200 trees/ha) than 1400_HD (1800 trees/ha), but elevation may have been a confounding factor.

3.5. Remote sensing of forest canopy

The remotely sensed canopy metrics exhibited great variability between the techniques used in this analysis (Tables 4- 6). The CANAPI-derived average tree heights were lower than tree heights estimated from TLS and the MISR SGM (Table 4). MISR heights were greater than the TLS estimates. Between 2011 and 2012, the MISR tree heights showed little variability and the average heights for the site the experienced a

burn between the two years, 1400_BU, actually decreased by very little. It was expected that following the fire, the average tree heights at this site would decrease considerably because many of the smaller trees were consumed in the high severity burn. However, there was not a forest inventory prior to the fire to confirm this.

Table 4. Tree heights (m) derived from TLS[a], CANAPI, and the MISR SGM[b]

	TLS heights (m)		CANAPI height (m)		2011 MISR height (m)		2012 MISR height (m)	
Site ID	Mean	St. Dev.	Mean	St. Dev.	Mean	St. Dev.	Mean	St. Dev.
1100_LD	-	-	10.1	7.9	16.1	0.5	15.9	0.6
1100_HD	-	-	10.3	6.9	14.6	1.0	14.3	0.4
1200_LD	-	-	6.8	4.4	16.1	0.4	15.8	0.4
1200_HD	-	-	9.7	8.7	15.0	0.6	15.0	0.5
1300_LD	-	-	7.6	5.1	16.9	1.1	-	-
1300_HD	-	-	9.9	7.1	-	-	-	-
1400_LD	11.6	4.6	6.2	3.7	-	-	16.6	0.7
1400_HD	10.6	3.7	6.0	3.6	18.5	3.8	16.4	0.0
1400_BU	13.3	5.1	6.4	3.7	16.2	0.5	15.1	0.7
1550_LD	-	-	4.4	2.5	-	-	16.6	0.6

[a]TLS tree heights were only determined for the three sites at 1400 m.
[b]The MISR reflectance data resulted in singular matrices that could not be inverted in the SGM, so canopy metrics were not derived for 1300_HD, 1400_LD, and 1550_LD using 2011 data and for 1300_LD and 1300_HD sites using 2012 data.

Crown radii estimated from CANAPI were much greater than for either TLS or the MISR SGM for 2011 or 2012 (Table 5). The site average crown radii were slightly lower for the TLS derived estimates than the MISR estimates. Again the MISR SGM resulted in little variability between years even for 1400_BU.

The CANAPI results showed tree densities that were greater than TLS estimates and MISR estimates (Table 6). The MISR SGM estimates presented great variability that did not correspond to the density classifications of each site. For instance, the 2011

MISR SGM returned a greater tree density for 1100_LD than 1100_HD (540 trees/ha versus 30 trees/ha) and similarly a greater tree density for 1200_LD than 1200_HD (440 trees/ha versus 20 trees per/ha). The results were similar for the 2012 data.

Table 5. Tree crown radii (m) derived from TLS, CANAPI, and the MISR SGM

	TLS crown radius (m)		CANAPI crown radius (m)		2011 MISR crown radius (m)		2012 MISR crown radius (m)	
Site ID	Mean	St. Dev.	Mean	St. Dev.	Mean	St. Dev.	Mean	St. Dev.
1100_LD	-	-	3.3	1.8	1.8	0.06	2.0	0.05
1100_HD	-	-	3.8	2.0	2.0	0.13	1.8	0.09
1200_LD	-	-	2.9	1.7	2.0	0.03	2.0	0.04
1200_HD	-	-	2.9	1.6	1.9	0.07	1.9	0.07
1300_LD	-	-	3.4	1.9	2.1	0.13	-	-
1300_HD	-	-	3.8	2.0	-	-	-	-
1400_LD	0.8	0.4	3.2	1.9	-	-	2.0	0.18
1400_HD	1.0	0.3	2.9	1.7	2.3	0.94	2.1	0.0
1400_BU	1.5	0.6	3.0	1.8	2.0	0.05	1.9	0.39
1550_LD	-	-	2.0	1.0	-	-	2.1	0.07

Table 6. Tree density (trees/ha) derived from TLS, CANAPI, and the MISR SGM[a]

			2011 MISR density (trees/ha)		2012 MISR density (trees/ha)	
Site ID	TLS density (trees/ha)	CANAPI density (trees/ha)	Mean	St. Dev.	Mean	St. Dev.
1100_LD	-	1200	540	570	460	140
1100_HD	-	1900	30	30	30	10
1200_LD	-	1600	440	210	140	100
1200_HD	-	1400	20	5	40	30
1300_LD	-	1900	1250	1010	-	-
1300_HD	-	2100	-	-	-	-
1400_LD	550	1700	-	-	540	440
1400_HD	3000	1700	50	40	800	0
1400_BU	1400	1800	190	110	460	170
1550_LD	-	70	-	-	300	160

[a]Data from multiple MISR orbits were averaged to determine tree density, while data from only one dataset was used to generate density from the TLS data and CANAPI SGM.

There was not a significant relationship established between the field measured tree heights and the estimates from the remote sensing techniques (Figure 13a). However, the field measured site averages do not cover a sufficient spread of tree heights to establish a scaling relationship with the remote sensing techniques. For instance, most of the sites have an average tree height between 5 and 15 m. The CANAPI algorithm underestimated all field measured heights and the MISR SGM overestimated all heights except for the sites with the tallest trees. The SGM underestimated tree heights for these sites. TLS slightly overestimated average heights for the three 1400 m plots, but the average height was overestimated the most at 1400_BU.

The two SGM models both overestimated crown radius compared to the field surveys except for the sites with the largest trees (Figure 13b). The crown radii modeled by CANAPI indicated no obvious trend with most values occurring in a range 2.9 to 3.4 m. Field surveys indicated that few of the sites had average crown radii within that range. The MISR SGM modeled values show a similar pattern to those from CANAPI, indicating that the crowns for all field sites were about the same size. However MISR SGM modeled crowns better represented field values for small crown radii. Average crown radii from the TLS data provided fair estimates for 1400_HD and 1400_LD but overestimated radii for 1400_BU. Branches on the standing dead trees at this recently burned site were likely detected as crown in the canopy delineation algorithm but may not have been included in the field inventory. Most remaining branches would have been at the top of the tree making ground crown measurements difficult and subjective.

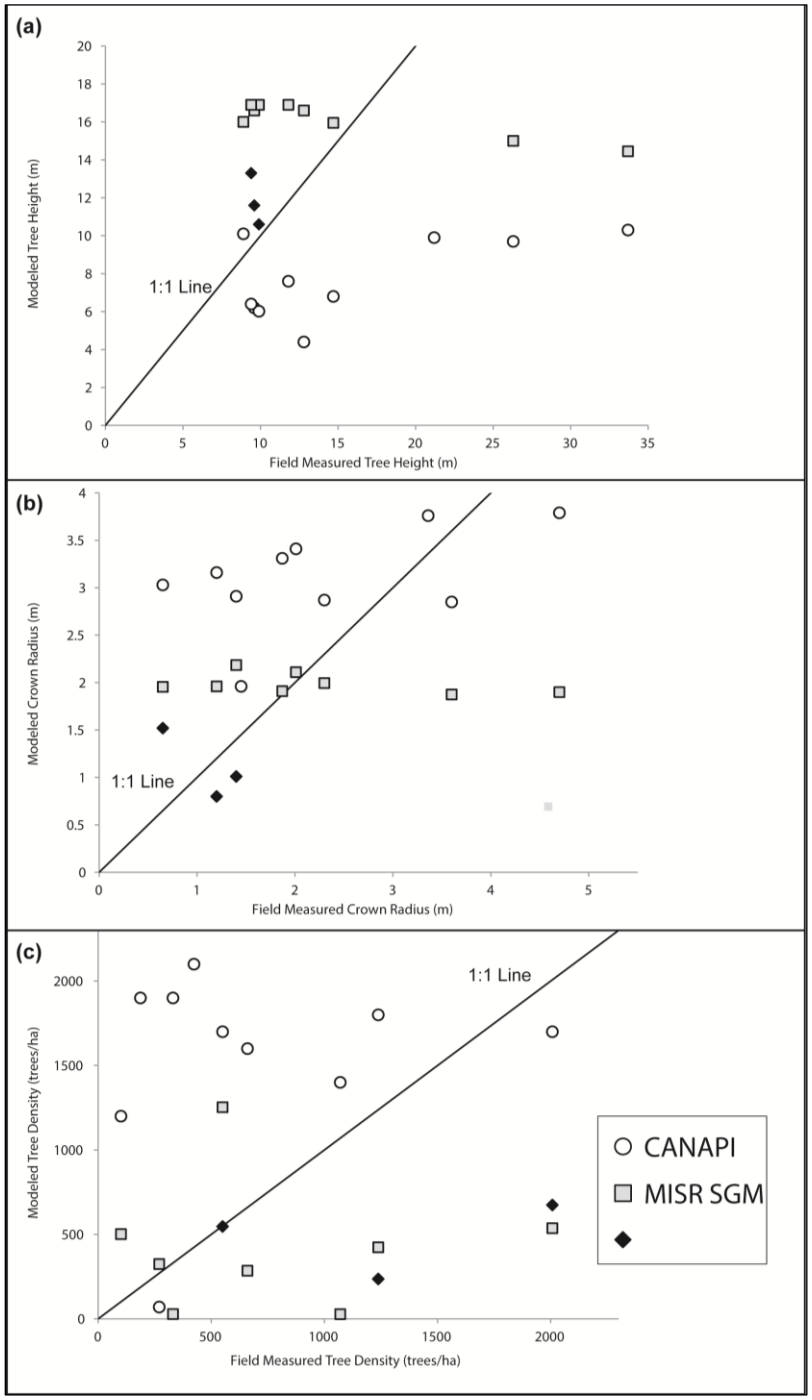

Figure 13. Canopy metrics derived from TLS, the CANAPI SGM, and MISR SGM plotted against field measured values of tree height (a), crown radius (b), and tree density (c).

There may be a stronger relationship between CANAPI-modeled tree density compared to the other metrics, however it shows a large positive bias (over-predicts for almost all ground density values) (Figure 13c). The MISR SGM again indicated a relatively small range of tree densities for the given range of field measured values, however it was very close to the TLS measured values for 1400_HD and 1400_LD. TLS tended to underestimate field measured tree density suggesting that the thresholds used in the canopy automation process may be missing trees that were included in the field survey. However, it is possible that sample bias during the forest inventory influenced these data values. For all metrics, CANAPI and the MISR SGM failed to identify the sites that exhibited the highest or lowest canopy parameters, indicating that model improvement must occur before these methods can effectively be implemented in a canopy adjustment.

As TLS was only collected at three plots, it was difficult to determine if this method would provide accurate and unbiased measurements of average tree height and crown radius for site canopy characterization. Therefore, all estimated tree heights and crown radii from the TLS scan plots were compared to all field measured values in the 1400 m sites (Figure 14a-c). Because these samples were taken from the same population and were subsequently not independent, the non-parametric Wilcoxon signed-rank test was selected to test for significant differences ($\alpha = 0.05$) between the median tree height and crown radius determined from each measurement method.

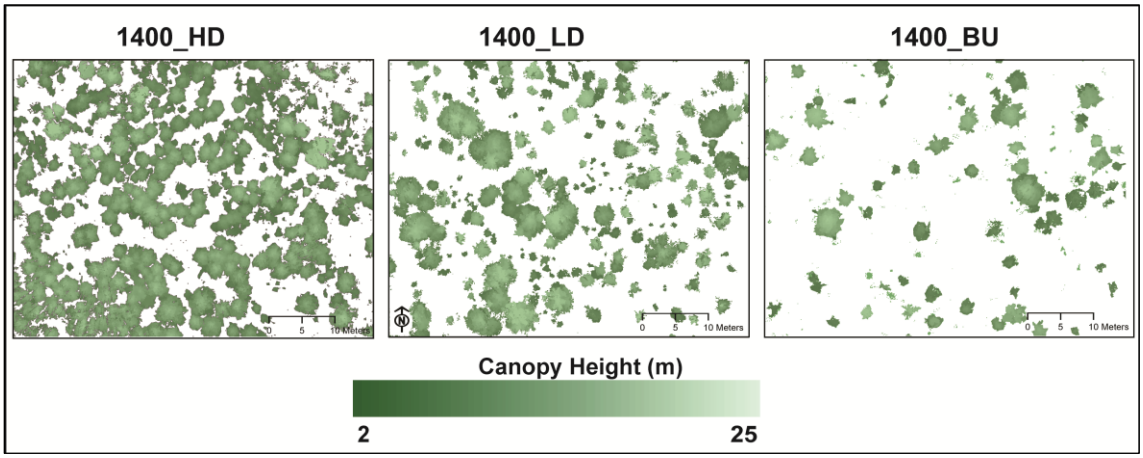

Figure 14. The tree canopy extents and height delineated from TLS data for 1400_HD (a), 1400_LD (b), and 1400_BU (c).

TLS determined crown radius were significantly different than the field measured crown radii at all three sites. Field measured crowns were consistently lower for 1400_HD and 1400_LD than the TLS measured values, but in 1400_BU the field measure values were much lower than TLS derived crowns (Figure 15d-f). This suggests that the canopy delineation algorithm was considering branches to be a part of the crown that field inventories were not. Tree heights at 1400_BU and 1400_HD were not significantly different from field measured values, but heights at 1400_LD site were. Although the difference was not significant for 1400_HD and 1400_LD, mean field measured heights were slightly lower than TLS heights for all sites (Figure 15a-c). This may indicate some bias in the TLS height detection algorithm given that field measured heights were accurately obtained.

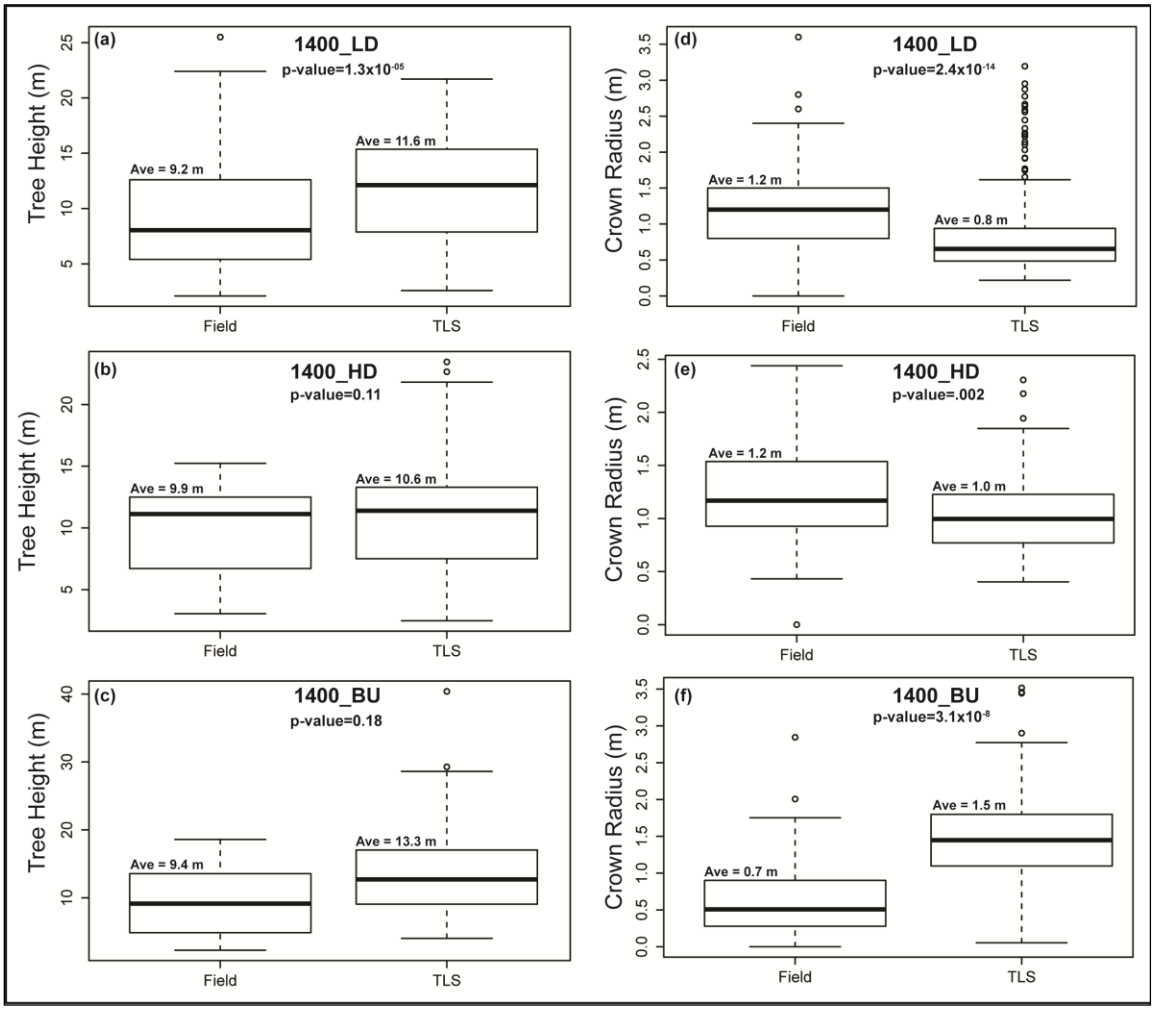

Figure 15. Box plots for TLS and field measured tree heights (a-c) and crown radii (d-f) at the 1400 m sites.

Chapter 4. Discussion

4.1. How well does the *f*SCA observable by satellites approximate sub-canopy *f*SCA?

The purpose of this study was to assess a canopy adjustment for satellite fractional snow-covered area. Therefore, the first research question was posed to test the primary assumption inherent in the currently employed canopy adjustment: that snow in sub-canopy locations follows the distribution of snow in canopy openings. It was anticipated that evidence against this assumption would be manifested in the differences between $f\text{SCA}_{\text{ADJ}}$ and $f\text{SCA}_{\text{GROUND}}$, subsequently indicating where the vegetation fraction canopy adjustment performs well and where it does not properly represent sub-canopy snow cover. While $f\text{SCA}_{\text{ADJ}}$ was established as an improvement over $f\text{SCA}_{\text{TM}}$, it was demonstrated that there remains considerable error between $f\text{SCA}_{\text{ADJ}}$ and $f\text{SCA}_{\text{GROUND}}$ during late season snowmelt.

There was a distinct difference between snow in open and sub-canopy locations, both between and within study sites in the central Oregon Cascades. These differences lead to errors of commission when snow exists in openings adjacent to snow-free, sub-canopy locations, and lead to errors of omission in locations where there is insufficient snow in canopy gaps to be detected by TMSCAG. These misrepresentations of $f\text{SCA}_{\text{GROUND}}$, are not ubiquitous and vary depending on time of year, elevation, and canopy characteristics.

4.2. What spatio-temporal snow cover patterns explain differences between in situ snow cover and satellite *f*SCA?

Snow observations demonstrate that differences between $fSCA_{ADJ}$ and $fSCA_{GROUND}$ are a result of varying snow cover dynamics between sub-canopy and open locations, not errors in the snow detection algorithm. The rapid depletion of *in situ* observed snow cover at 1300_HD provides evidence for the large error of commission at this site on 14 May. At 1400_HD, observations confirmed that the errors of omission present on 15 June occurred because late season snow was primarily retained in undetectable, sub-canopy locations. A similar snow cover depletion trend between this and the 1500_HD site, suggest that the same pattern is responsible for the errors of omission at 1500_HD. In contrast, during advanced melt, the snow fraction was greater for open locations at 1400_LD, causing an overestimate of $fSCA_{GROUND}$ on 14 May. These discontinuities between observable and sub-canopy snow, which lead to errors in $fSCA_{ADJ,}$ can be explained by plausible physical process linked to both elevation and canopy characteristics.

The early disappearance of sub-canopy snow at 1300_HD may be associated with the interception efficiency of the large trees that are dominant at this site, coupled with warmer temperatures experienced at low elevations. It has been reported that up to 60% of snowfall can be intercepted by forest canopies in the Oregon Cascades, and for low elevation forests, as much as 70% of intercepted snow will melt from the tree canopy before reaching the ground [*Storck et al*., 2002]. Recent work shows that about 40-50% of snowfall is intercepted by forest canopy at the forested sites used in this analysis [*Roth and Nolin*, unpublished]. The 1300 m sites are situated just above the rain-snow transition

zone and are frequently subject to temperatures slightly above freezing. Temperature data from an adjacent meteorological station indicated that the average daily temperatures were greater than 1°C for 46% of the 119 days between January and April. Daily maximum temperatures of at least 8°C were observed on 21 days during this time period and daily minimum temperatures failed to reach freezing on 45 days. With temperatures hovering at or just above 0°C at the 1100 m, 1200 m, and 1300 m sites, it is reasonable that a considerable portion of the intercepted snow melted from the canopy before it had a chance to accumulate under the trees. Additionally, although sublimation is not a major contributing factor for snow loss from tree canopies in the humid, temperate climate of the Oregon Cascades [*Storck et al*., 2002], it may exhibit a greater influence at lower elevations [*Montesi et al*., 2004].

The persistence of snow cover in sub-canopy locations relative to canopy openings at 1400_HD and 1500_HD is indicative of the colder temperatures that occur at high elevations combined with the solar shading provided by the dense, continuous forest canopy [*Metcalfe and Buttle*, 1998; *Musselman et al*., 2008]. Despite having moderate tree cover (600 trees/ha), 1400_LD did not experience a similar pattern. The forest at this site is characterized by clumps of trees rather than continuous cover of evenly distributed trees. During the final 14 days of persisting snow cover at this site, the sub-canopy snow fraction was between 20 % and 35 % lower under the clumps of trees than the snow fraction in gaps, indicating that shading and reduced turbulent fluxes under clumps of trees did not offset the increased interception and enhanced longwave radiation provided by the canopy [*Musselman et al*., 2008; *Ellis et al., 2011*]. Additionally, the size of inter-

clump gaps at 1400_LD may be small enough to allow sufficient forest shading along the gap margins to retard melt rates compared to a large forest opening [*Berry and Rothwell*, 1992].

The hydrologic significance of the errors of commission and omission by $f\mathrm{SCA}_{\mathrm{ADJ}}$ were investigated by analyzing snow surveys of SWE and snow depth measurements at two of the study sites. One snow survey performed at 1500_HD on 15 June showed that underestimated SWE resulting from errors of omission represented only 1% of the maximum annual SWE for that site. Therefore, the hydrologic implications associated with errors of omission at high elevations late in the snowmelt season may be small. This is reassuring because this type of error (underestimating sub-canopy snow) cannot be addressed with optical remote sensing techniques.

Alternatively, the 70% over prediction of snow cover at 1300_HD may have greater hydrologic implications. A snow survey conducted at this site on May 15 indicated that average SWE was about 1 m in the adjacent low-density site. If this same snow cover was assumed to be present over 70% of the area encompassed by the 1300_HD forest, these projections would lead to the assumption that 40% of the maximum annual SWE was remaining. Errors of commission (overestimating sub-canopy snow) do, however, have the potential to be reduced with the incorporation of forest canopy characteristics to parameterize sub-canopy snow.

4.3. What specific canopy structure metrics account for differences between snow cover and satellite *f*SCA?

Field observations suggest that canopy interception and solar shading of snow are key processes that affecting differences between snow in sub-canopy and open locations observed in this study. Although interception and shading are moderated by forest canopy, a relationship could not be established to parameterize sub-canopy snow with canopy closure, tree height, crown radius, or tree density. The error in $fSCA_{ADJ}$ did not exhibit a distinct pattern with any one of these metrics. The most obvious pattern occurred for 24 February crown radius (Figure 12g) where the highest error occurred for high crown radii, but this relationship was not transferable to other dates.

Several limitations prohibited an adequate comparison of $fSCA_{ADJ}$ error and canopy structure. Foremost was the inability to acquire a sufficient time series of *f*SCA from TMSCAG. The combination of frequent cloudiness over the Oregon Cascades and 16-day cycle of Landsat 7 resulted in only three dates of TMSCAG data for comparison with *in situ* snow observations. These three dates were separated by considerable lengths of time (80 days between the first two and 32 days between the second two dates). This caused the snowmelt period to be completely missed at the 1100 m and 1200 m sites and prevented a thorough temporal investigation into the onset of increased error in $fSCA_{ADJ.}$ This also resulted in a limited data set, inhibiting the ability to examine inter-site differences of *f*SCA at low elevations.

The small range of canopy characteristics captured at each elevation further restricted the potential to discern relationships between forest canopy structure and error in $fSCA_{ADJ}$. For instance, there were no high elevation sites that had tall trees with large

crowns comparable to the low elevation sites exhibiting these characteristics. The study sites also failed to represent forest sites with short, small trees that may be less likely to necessitate a canopy adjustment. Additionally, the contrasting temporal patterns in SF_O and SF_{SC} at the 1400 m sites indicate that differences between snow cover in sub-canopy and open locations are controlled by an intricate combination of canopy metrics, including, but not necessarily limited to, canopy closure and tree density. Finally, these results are all founded on the assumption that the *in situ* snow observations and forest inventory measurements adequately represent site characteristics and capture the spatial variability needed to define inferential relationships. It is possible that sample bias and/or inadequate sampling introduced error in the results that could not be separated from error in $fSCA_{ADJ}$.

4.4. What remote sensing techniques can be used to represent field measured forest canopy structure at the landscape scale?

An adequate relationship was not determined between canopy structure from field measurements, TLS, aerial photography, and satellite reflectance data. Thus the ability to scale canopy structure to landscape estimates remains a challenge. TLS was able to accurately depict plot-scale forest canopy, but CANAPI and MISR SGM results did not give sufficiently accurate estimates of forest characteristics. This suggests that these models need to be refined to capture the range of canopy characteristics present in the Oregon Cascades.

Despite providing an adequate representation of tree heights and crown radii, the TLS canopy delineation algorithm can be improved. Tree density tended to be

underestimated by TLS in this study, suggesting that thresholds used to exclude ground cover and erroneous crowns may eliminate some small trees in the scan area that were inventoried in the field. Also, filtering the canopy heights to remove secondary peaks within a single tree crown may result in merging smaller tree canopies [*Koch et al.*, 2006]. A different method may also be necessary for burned sites where the full canopy depicted by TLS does not represent the sparse canopy of a dead tree.

Other possible sources of error in the TLS data are related to site-specific characteristics. High tree density limits the range of TLS, and dense undergrowth may prohibit the ability to accurately classify the ground surface [*Pirotti, et al*., 2012]. While this was not a problem at 1400_BU plot, it may have been an issue at 1400_HD and 1400_LD. TLS may also miss the peaks of tall trees and those close to the scanner where the TLS point cloud becomes less dense *[Hopkinson et al*., 2004a].

A couple of factors may be responsible for the misrepresentations of forest structure by the CANAPI algorithm. First, CANAPI tends to underestimate the height of tall trees and overestimate the height of small trees in heterogeneous stands. Also, tree heights and crown radii are not accurately estimated in high-density forests because discrete crowns cannot be detected in clumped canopies or where shadows are truncated by adjacent trees [*Chopping*, 2011]. It appears that groups have trees may have been aggregated into a single crown measurement at many of the sites in this study because CANAPI typically overestimated crown radii.

The MISR SGM may have failed to return reasonable canopy metrics for the same reasons that CANAPI produced erroneous results. In addition, the SGM cannot

accurately depict tree heights or delineate crowns in dense forests [*Chopping et al*., 2009]. Subsequently, the dense forests of the Oregon Cascades presents a challenge for canopy characterization with the SGM.

The limited range of values for forest canopy structure estimated by CANAPI and the MISR SGM also inhibited the ability to discern relationships between the remote sensing techniques and field measurements of canopy structure. These SGM's require user-defined values for background albedo that can provide adequate contrast between the ground and forest canopy to determine variability in the canopy structure [*Chopping et al.*, 2009; *Chopping et al*., 2012]. In this study, while the background albedo was determined properly, the dark background did not provide enough contrast in the dense forests to discern the three-dimensional canopy structure. Implementing the SGM's when snow is present under the forest canopy has the potential to improve the model performance in dense forests because the albedo of snow can be accurately quantified and provides high contrast background conditions [*Chopping et al*., 2009].

Finally, estimating forest canopy metrics at coarser scales may require more extensive field data collection for validation. Our conventional ground-based measurements of forest properties were limited to those trees located along a single transect passing through each study site. It may be unjustified to assume that this transect captures the variability that will be detected by TLS, aerial photography, or satellite remote sensing.

Chapter 5. Conclusions

The current canopy adjustment applied to *f*SCA from TMSCAG performs well when snow cover is homogenously distributed in open and forested areas. Errors that do occur during such times are limited to dense forests where the viewable gap fraction is too low to detect any snow cover. Once the viewable snow cover displays spatial variability in the gaps, the snow cover obscured by the canopy begins to differ from that in the open. These differences appear to depend on elevation, which acts as a proxy for temperature. Such differences decrease the accuracy of $fSCA_{ADJ}$ and demonstrate the need for further investigation to develop a more consistently accurate canopy adjustment. Our preliminary results show that the hydrologic implications of the errors may be small for high elevation snowpack but are more substantial for lower elevations where the area of snow cover is large and hence the cumulative error can be substantial.

While several limitations in this study prohibited the ability to quantify relationships between forest structure and sub-canopy snow, they provide direction for future improvements. Progress towards an effective canopy adjustment will require a continuous record of spatially coincident satellite-derived and *in situ* snow cover for varying forest densities. Miniature (iButton) temperature sensors were not successful in this study but have been presented as a novel method to track the spatial variability of snow cover without extensive field monitoring [*Lundquist and Lott*, 2008; *Raleigh et al*., 2013]. Strategic deployment of these sensors in a representative range of forest types, to monitor snow cover across multiple elevations, provides the means to separate these confounding variables. Combined with detailed forest canopy structure from ground-

based (TLS) or airborne LiDAR, these temperature sensors would offer key spatially distributed *f*SCA information at the plot scale. Though not available for this study, airborne LiDAR [*Hilker et al*., 2012] and satellite LiDAR from NASA's Geoscience Laser Altimeter System (GLAS) [*Sun et al.*, 2008] have the potential to provide cross-scale analysis of vegetation structure that can link plot scale estimates to landscape scale SGM estimates from aerial photos and MISR.

These *f*SCA and vegetation data products will provide the opportunity to further investigate spatial and temporal snow cover patterns in forested regions and help identify the canopy structure metrics that are needed to parameterize sub-canopy snow across spatial scales. They also provide the ability to characterize other canopy structure metrics that may influence snow cover patterns such as tree clump size and spacing. Studies including continuous snow cover measurements and vegetation remote sensing would need to be extended to other locations through coordinated campaigns in both maritime and continental snow climates, including Alaska's boreal forests and the Rocky Mountain West, to develop a universally applicable operational canopy adjustment.

Physically based snow models may prove to be a useful addition to a satellite *f*SCA canopy adjustment. Models, such as *Liston and Elder's* [2006] spatially distributed snow evolution model, SnowModel, evaluate snow-vegetation interactions and can provide insight into the snow accumulation and ablation processes that may have been responsible for the errors of commission and omission in this study. Incorporating all the tools at hand, including physical models, *in situ* snow and vegetation observations,

and remote sensing data can help elucidate the spatio-temporal snow cover patterns necessary for developing a universal canopy adjustment.

Once variability in snow cover can be assessed using readily quantifiable canopy metrics then we can start to address scaling issues in mapping *f*SCA from different platforms and in forested regions with substantial snow cover such as the Pacific Northwest mixed conifer forests and Northern Hemisphere boreal forests. This study indicates that the CANAPI and MISR SGM algorithms require refinement to perform more reliably in dense forests, but they remain viable options for estimating landscape forest structure from relatively easily attainable data.

The goal of monitoring global snow cover by VIIRS will depend on an effective accounting method for sub-canopy snow. This will be a multistep process beginning with proper parameterization of sub-canopy snow by forest canopy metrics, followed by the scaling of forest structure parameters to moderate resolutions and inclusion of these metrics to account for areas where the vegetation fraction adjustment is misrepresenting sub-canopy snow. Moderate resolution canopy metrics can then be used to improve canopy adjustments for VIIRS, along with other moderate resolution snow products.

While the initial goal in this study is an accurate canopy adjustment for optical remote sensing of *f*SCA, this is a step along the way to overall improvements in snow remote sensing for all sensor types. It is anticipated that an approach using satellite observations of snow cover and forest canopy combined with process-based snow modeling will provide us with the cross-scale spatial and temporal snow characterization needed for hydrologic and climatologic applications including the monitoring of snow

cover and subsequent hydrologic response in climate sensitive regions, such as the Oregon Cascades.

References

Abatzoglou, J.T. (2011), Influence of the PNA on declining mountain snowpack in the Western United States. *International Journal of Climatology, 31*(8), 1135-1142, doi: 10.1002/joc.2137.

Anderton, S.P., White, S.M. and Alvera, B. (2004), Evaluation of spatial variability in snow water equivalent for a high mountain catchment. *Hydrological Processes, 18*(3), 435-453, doi: 10.1002/hyp.1319.

Baker, N. (2011), Joint Polar Satellite System (JPSS) VIIRS Snow Cover Algorithm Theoretical Basis Document (ATBD). pp. 1-52, Northrop Grumman Aerospace Systems, Redondo Beach, CA.

Berry, G.J. and Rothwell, R.L. (1992), Snow ablation in small forest openings in Southwest Alberta. *Canadian Journal of Forest Research, 22*(9), 1326-1331.

Blöschl, G. and Kirnbauer, R. (1992), An analysis of snow cover patterns in a small alpine catchment. *Hydrological Processes,* 6(1), 99-109, doi: 10.1002/hyp.3360060109

Brown, R.D. and Mote, P.W. (2009), The response of northern hemisphere snow cover to a changing climate. *Journal of Climate, 22*(8), 2124-2145, doi: 10.1175/2008jcli2665.1.

Butt, M.J. and Bilal, M. (2011), Application of snowmelt runoff model for water resource management. *Hydrologic Processes, 25,* 3735-3747, doi: 10.1002/hyp.8099.

Chen, J.M. and Cihlar, J. (1996), Retrieving leaf area index of boreal conifer forests using Landsat TM image*., Remote Sensing of Environment, 55*(2), 153-162, doi: 10.1016/0034-4257(95)00195-6.

Chopping, M. (2011), CANAPI: canopy analysis with panchromatic imagery. *Remote Sensing Letters, 2*(1), 21-29, doi: 10.1080/01431161.2010.486805.

Chopping, M., Nolin, A., Moisen, G.G., Martonchik, J.V. and Bull, M. (2009), Forest canopy height from the Multiangle Imaging SpectroRadiometer (MISR) assessed with high resolution discrete return lidar. *Remote Sensing of Environment, 113*(10), 2172-2185, doi: 10.1016/j.rse.2009.05.017.

Chopping, M., North, M., Jiquan, C., Schaaf, C.B., Blair, J., Martonchik, J.V. and Bull, M.A. (2012), Forest canopy cover and height from MISR in topographically complex southwestern US landscapes assessed with high quality reference data. *IEEE Journal of Selected Topics in Applied Earth Observations and Remote Sensing, 5*(1), 44-58, doi: 10.1109/jstars.2012.2184270.

Clark, M.P., Slater, A.G., Barrett, A.P., Hay, L.E., McCabe, G.J., Rajagopalan, B. and Leavesley, G.H. (2006), Assimilation of snow covered area information into hydrologic and land-surface models. *Advances in Water Resources, 29*(8), 1209-1221, doi: 10.1016/j.advwatres.2005.10.001.

Davis, R.E., Hardy, J.P., Ni, W., Woodcock, C., McKenzie, J.C., Jordan, R. and Li, X. (1997), Variation of snow cover ablation in the boreal forest: A sensitivity study on the effects of conifer canopy. *Journal of Geophysical Research, 102*(D24), 29389-29395, doi: 10.1029/97jd01335.

Diner, D.J., Asner, G.P., Davies, R., Knyazikhin, Y., Muller, J.P., Nolin, A.W., Pinty, B., Schaaf, C.B. and Stroeve, J. (1999), New directions in earth observing: Scientific applications of multiangle remote sensing. *Bulletin of the American Meteorological Society, 80*(11), 2209-2228, doi: 10.1175/1520-0477(1999)080<2209:ndieos>2.0.co;2.

Dozier, J. (2011), Mountain hydrology, snow color, and the fourth paradigm. Eos, Transactions *American Geophysical Union, 92*(43), 373-374, doi: 10.1029/2011eo430001

Dozier, J. (1989), Spectral signature of alpine snow cover from the Landsat Thematic Mapper. *Remote Sensing of Environment, 28*(April-June), 9-22.

Dozier, J., Painter, T.H., Rittger, K. and Frew, J.E. (2008), Time–space continuity of daily maps of fractional snow cover and albedo from MODIS. *Advances in Water Resources, 31*(11), 1515-1526, doi: 10.1016/j.advwatres.2008.08.011.

Elder, K., Rosenthal, W. and Davis, R.E. (1998), Estimating the spatial distribution of snow water equivalence in a montane watershed. *Hydrological Processes, 12*(10-11), 1793-1808, doi: 10.1002/(sici)1099-1085(199808/09)12:10/11<1793::aid-hyp695>3.0.co;2-k.

Ellis, C.R., Pomeroy, J.W., Essery, R.L.H. and Link, T.E. (2011), Effects of needleleaf forest cover on radiation and snowmelt dynamics in the Canadian Rocky Mountains. *Canadian Journal of Forest Research, 41*(3), 608-620, doi: 10.1139/X10-227.

Elzinga, C.L., Salzer, D.W. and Willoughby, J.W. (1998), Measuring and monitoring plant populations. Technical reference 1730-1. Bureau of Land Management. Management, Denver, Colorado.

Faria, D.A., Pomeroy, J.W. and Essery, R.L.H. (2000), Effect of covariance between ablation and snow water equivalent on depletion of snow-covered area in a forest. *Hydrological Processes, 14*(15), 2683-2695, doi: 10.1002/1099-1085(20001030)14:15<2683::aid-hyp86>3.0.co;2-n.

Fletcher, C.G., Kushner, P.J., Hall, A. and Qu, X. (2009), Circulation responses to snow albedo feedback in climate change. *Geophysical Research Letters, 36*(9), L09702, doi: 10.1029/2009gl038011.

Frazer, G.W., Canham, C.D. and Lertzman, K.P. (1999), Gap Light Analyzer (GLA), Version 2.0: Imaging software to extract canopy structure and gap light transmission indices from true-colour fisheye photographs, users manual and program documentation, Simon Fraser University, Burnaby British Columbia, Institute of Ecosystem Studies, Milibrook, New York.

Golding, D.L. and Swanson, R.H. (1986), Snow distribution patterns in clearings and adjacent forest. *Water Resources Research, 22*(13), 1931-1940, doi: 10.1029/WR022i013p01931.

Hall, D.K. and Riggs, G.A. (2007), Accuracy assessment of the MODIS snow products. *Hydrological Processes, 21*(12), 1534-1547, doi: 10.1002/hyp.6715.

Hilker, T., Coops, N.C., Newnham, G.J., van Leeuwen, M., Wulder, M.A. Stewart, J. and Culvenor, D.S. (2012), Comparison of terrestrial and airborne LiDAR in describing stand structure of a thinned lodgepole pine forest. *Journal of Forestry, 110*(2), 97-104, doi: 10.5849/jof.11-003.

Hilker, T., Leeuwen, M., Coops, N., Wulder, M., Newnham, G., Jupp, D.B. and Culvenor, D. (2010), Comparing canopy metrics derived from terrestrial and airborne laser scanning in a Douglas-fir dominated forest stand. *Trees, 24*(5), 819-832, doi: 10.1007/s00468-010-0452-7.

Hinkler, J., Pedersen, S.B., Rasch, M. and Hansen, B.U. (2002), Automatic snow cover monitoring at high temporal and spatial resolution, using images taken by a standard digital camera. *International Journal of Remote Sensing, 23*(21), 4669-4682, doi: 10.1080/01431160110113881.

Hopkinson, C., Chasmer, L., Colin, Y.-P. and Treitz, P. (2004a), Assessing forest metrics with a ground-based scanning lidar. *Canadian Journal of Forest Research, 34*(3), 573-583, doi: 10.1139/x03-225.

Hopkinson, C., Sitar, M., Chasmer, L. and Treitz, P. (2004b), Mapping snowpack depth beneath forest canopies using airborne lidar. *Photogrammetric Engineering and Remote Sensing, 70*(3), 323-330.

Inoue, A., Yamamoto, K., Mizoue, N. and Kawahara, Y. (2004), Calibrating view angle and lens distortion of the Nikon fish-eye converter FC-E8. *Journal of Forest Research, 9*(2), 177-181, doi: 10.1007/s10310-003-0073-8.

Jefferson, A.J. (2011), Seasonal versus transient snow and the elevation dependence of climate sensitivity in maritime mountainous regions. *Geophysical Research Letters, 38*(L16402), 1-7, doi: 10.1029/2011GL048346.

Jin, Y., Randerson, J.T., Goulden, M. L., and Goetz, S.J. (2012), Post-fire changes in net shortwave radiation along a latitudinal gradient in boreal North America. *Geophysical Research Letters, 39*(13), L13403, doi:10.1029/2012GL051790.

Kerr, T., Clark, M., Hendrikx, J. and Anderson, B. (2013), Snow distribution in a steep mid-latitude alpine catchment. *Advances in Water Resources, 55*, 17-24, doi: 10.1016/j.advwatres.2012.12.010.

Klein, A.G., Hall, D.K. and Riggs, G.A. (1998), Improving snow cover mapping in forests through the use of a canopy reflectance model. *Hydrological Processes, 12*(10-11), 1723-1744, doi: 10.1002/(sici)1099-1085(199808/09)12:10/11<1723::aid-hyp691>3.0.co;2-2.

Koch, B., Heyder, U. and Weinacker, H. (2006), Detection of individual tree crowns in airborne lidar data. *Photogrammetric Engineering and Remote Sensing, 72*(4), 357-363.

Lee, S., Klein, A.G., and Over, T.M. (2005), A comparison of MODIS and NOHRSC snow-cover products for simulating streamflow using Snowmelt Runoff Model. *Hydrological Processes, 19*, 2951-2972, doi: 10.1002/hyp.5810.

Link, T. and Marks, D. (1999), Distributed simulation of snowcover mass- and energy-balance in the boreal forest. *Hydrological Processes, 13*(14-15), 2439-2452, doi: 10.1002/(sici)1099-1085(199910)13:14/15<2439::aid-hyp866>3.0.co;2-1.

Liston, G.E., and Elder, K. (2006), A distributed snow-evolution modeling system (SnowModel). *Journal of Hydrometeorology, 7*(6), 1259-1276, doi: 10.1175/JHM548.1.

López-Moreno, J.I. and Latron, J. (2008), Influence of canopy density on snow distribution in a temperate mountain range. *Hydrological Processes, 22*(1), 117-126, doi: 10.1002/hyp.6572.

Lundquist, J.D. and Lott, F. (2008), Using inexpensive temperature sensors to monitor the duration and heterogeneity of snow-covered areas. *Water Resources Research, 44*(W00D16), 1-6, doi: 10.1029/2008wr007035.

Maas, H.G., Bienert, A., Scheller, S. and Keane, E. (2008), Automatic forest inventory parameter determination from terrestrial laser scanner data. *International Journal of Remote Sensing, 29*(5), 1579-1593, doi: 10.1080/01431160701736406.

Marks, D., Kimball, J., Tingey, D. and Link, T. (1998), The sensitivity of snowmelt processes to climate conditions and forest cover during rain-on-snow: a case study of the 1996 Pacific Northwest flood. *Hydrological Processes, 12*(10-11), 1569-1587, doi: 10.1002/(sici)1099-1085(199808/09)12:10/11<1569::aid-hyp682>3.0.co;2-l.

Martinec, J., Rango, A. (1995), Seasonal runoff forecasts for hydropower based on remote sensing. *Proc. 63rd Annual Western Snow Conference, Sparks, Nevada,* (pp. 10-20).

Martinec, J., and Rango, A. (1986), Parameter values for snowmelt runoff modeling. *Journal of Hydrology, 85*, 197-219.

Martinec, J., and Rango, A. (2008), Snowmelt-Runoff Model (SRM) user's manual updated edition for Windows (WinSRM 1.11). USDA Jornada Experimental Range, New Mexico State University, Las Cruces, NM, USA.

McGuire, M., Wood, A., Hamlet, A. and Lettenmaier, D. (2006), Use of Satellite Data for Streamflow and Reservoir Storage Forecasts in the Snake River Basin. *Journal of Water Resources Planning and Management, 132*(2), 97-110, doi: 10.1061/(asce)0733-9496(2006)132:2(97).

Metcalfe, R.A. and Buttle, J.M. (1998), A statistical model of spatially distributed snowmelt rates in a boreal forest basin. *Hydrological Processes, 12*(10-11), 1701-1722, doi: 10.1002/(sici)1099-1085(199808/09)12:10/11<1701::aid-hyp690>3.0.co;2-d.

Molotch, N.P. and Margulis, S.A. (2008), Estimating the distribution of snow water equivalent using remotely sensed snow cover data and a spatially distributed snowmelt model: A multi-resolution, multi-sensor comparison. *Advances in Water Resources, 31*(11), 1503-1514, doi: 10.1016/j.advwatres.2008.07.017.

Montesi, J., Elder, K., Schmidt, R.A. and Davis, R.E. (2004), Sublimation of intercepted snow within a subalpine forest canopy at two elevations. *Journal of Hydrometeorology, 5*(5), 763-773, doi: 10.1175/1525-7541(2004)005<0763:soiswa>2.0.co;2.

Mote, P.W. (2006), Climate-driven variability and trends in mountain snowpack in western North America. *Journal of Climate, 19*(23), 6209-6220, doi: 10.1175/jcli3971.1.

Mote, P.W., Hamlet, A.F., Clark, M.P. and Lettenmaier, D.P. (2005), Declining Mountain Snowpack in Western North America. *Bulletin of the American Meteorological Society, 86*(1), 39-49, doi: 10.1175/bams-86-1-39.

Musselman, K.N., Molotch, N.P. and Brooks, P.D. (2008), Effects of vegetation on snow accumulation and ablation in a mid-latitude sub-alpine forest. *Hydrological Processes, 22*(15), 2767-2776, doi: 10.1002/hyp.7050.

National Aeronautics and Space Administration (2011), Landsat 7 Science Data Users Handbook. Greenbelt, MD, USA.

National Resource Conservation Service Snowpack Reports, http://www.or.nrcs.usda.gov/snow/data/historic.html, accessed May 2013.

Nolin, A.W. (2010), Recent advances in remote sensing of seasonal snow. *Journal of Glaciology, 56*(200), 1141-1150, doi: 10.3189/002214311796406077.

Nolin, A.W. and Daly, C. (2006), Mapping "at risk" snow in the Pacific Northwest. *Journal of Hydrometeorology, 7*(5), 1164-1171, doi: 10.1175/jhm543.1.

Nolin, A.W., Dozier, J. and Mertes, L.A.K. (1993), Mapping alpine snow using a spectral mixture modeling technique. *Annals of Glaciology, 17*, 121-124.

O'Halloran, T.L., Law, B.E., Goulden, M.L., Wang, Z., Barr, J.G., Schaaf, C., Brown, M., Fuentes, J.D., Göckede, M., and Black, A. (2012), Radiative forcing of natural forest disturbances. *Global Change Biology, 18*(2), 555-565.

Olsen, M., Johnstone, E., Kuester, F., Driscoll, N. and Ashford, S. (2011), New automated point-cloud alignment for ground-based light detection and ranging data of long coastal sections. *Journal of Surveying Engineering, 137*(1), 14-25, doi: doi:10.1061/(ASCE)SU.1943-5428.0000030.

Painter, T.H., Rittger, K., McKenzie, C., Slaughter, P., Davis, R.E. and Dozier, J. (2009), Retrieval of subpixel snow covered area, grain size, and albedo from MODIS. *Remote Sensing of Environment, 113*(4), 868-879, doi: 10.1016/j.rse.2009.01.001.

Pederson, G.T., Betancourt, J.L., McCabe, G.J. (2013), Regional patterns and proximal causes of the recent snowpack decline in the Rocky Mountains, U.S. *Geophysical Research Letters, 40*, 1-6, doi: 10.1002/grl.50424.

Pirotti, F., Grigolato, S., Lingua, E., Sitzia, T. and Tarolli, P. (2012), Laser scanner applications in forest and environmental sciences. *Italian Journal of Remote Sensing*, 44(1), 109-123, doi: 10.5721/ItJRS20124419.

Pomeroy, J.W., Gray, D.M., Hedstrom, N.R. and Janowicz, J.R. (2002), Prediction of seasonal snow accumulation in cold climate forests. *Hydrological Processes, 16*(18), 3543-3558, doi: 10.1002/hyp.1228.

Qu, X. and Hall, A. (2006), Assessing snow albedo feedback in simulated climate change. *Journal of Climate, 19*(11), 2617-2630, doi: 10.1175/jcli3750.1.

Raleigh, M.S., Rittger, K., Moore, C.E., Henn, B., Lutz, J.A. and Lundquist, J.D. (2013), Ground-based testing of MODIS fractional snow cover in subalpine meadows and forests of the Sierra Nevada. *Remote Sensing of Environment, 128*, 44-57, doi: 10.1016/j.rse.2012.09.016.

Randerson, J.T., Liu, H., Flanner, M.G., Chambers, S.D., Jin, Y., Hess, P.G., Pfister, G., Mack, M.C., Treseder, K.K., Welp, L.R., Chapin, F.S., Harden, J.W., Goulden,

M.L., Lyons, E., Neff, J.C., Schuur, E.A., and Zender, C.S. (2006), The impact of boreal forest fire on climate warming. *Science, 314*(5802), 1130-1132.

RIEGL Laser Measurement Systems, (2013), RIEGL VZ-400: 3D Terrestrial laser scanner with online waveform processing. Orland, Florida, (pp 1-2).

Rittger, K., Painter, T.H., Dozier, J. (2013), Assessment of methods for mapping snow cover from MODIS. *Advances in Water Resources, 51*, 367-380, doi: 10.1016/j.advwatres.2012.03.002.

Salomonson, V.V. and Appel, I. (2004), Estimating fractional snow cover from MODIS using the normalized difference snow index. *Remote Sensing of Environment, 8*9(3), 351-360, doi: 10.1016/j.rse.2003.10.016.

Schmidt, R.A. and Gluns, D.R. (1991), Snowfall interception on branches of three conifer species. *Canadian Journal of Forest Research, 21*(8), 1262-1269.

Seidel, D., Fleck, S. and Leuschner, C. (2012), Analyzing forest canopies with ground-based laser scanning: A comparison with hemispherical photography. *Agricultural and Forest Meteorology, 154*, 1-8, doi: 10.1016/j.agrformet.2011.10.006.

Shook, K., Gray, D.M., and Pomeroy, J.W. (1993), Temporal variation in snow cover area during melt in prairie and alpine environments. *Nordic Hydrology, 24*(2-3), 183-198.

Song, C. (2012), Optical remote sensing of forest leaf area index and biomass. *Progress in Physical Geography, 37*(1), 98-113, doi: 10.1177/0309133312471367

Stoelinga, M.T., Albright, M.D. and Mass, C.F. (2010), A new look at snowpack trends in the Cascade Mountains. *Journal of Climate, 23*(10), 2473-2491, doi: 10.1175/2009jcli2911.1.

Storck, P. (2002), Measurement of snow interception and canopy effects on snow accumulation and melt in a mountainous maritime climate, Oregon, United States. *Water Resources Research, 38*(11), doi: 10.1029/2002wr001281.

Sturm, M. (1992), Snow distribution and heat flow in the Taiga. *Arctic and Alpine Research, 24*(2), 145-152.

Sun, G., Ranson, K.J., Kimes, D.S., Blair, J.B., Kovacs, K. (2008), Forest vertical structure from GLAS: An evaluation using LVIS and SRTM data. *Remote Sensing of Environment, 112*(2008), 107-117, doi: 10.1016/j.rse.2006.09.036.

Tague, C. and Grant, G.E. (2004), A geological framework for interpreting the low-flow regimes of Cascade streams, Willamette River Basin, Oregon. *Water Resources Research, 40*(4), doi: 10.1029/2003wr002629.

Thirel, G., Salamon, P., Burek, P., Kalas, M. (2011), Assimilation of MODIS snow cover area data in a distributed hydrologic model. *Hydrology Earth System Sciences Discussions, 8*, 1329-1364, doi: 10.5194/hessd-9-1329-2011.

Trujillo, E., Ramírez, J.A. and Elder, K.J. (2007), Topographic, meteorologic, and canopy controls on the scaling characteristics of the spatial distribution of snow depth fields. *Water Resources Research, 43*(7), doi: 10.1029/2006wr005317.

USGS (2013), Landsat ETM+ SLC-off - Path: 29 Row: 30 for Scene: LE70290302013073EDC00. U.S. Geological Survey, USGS Earth Resources Observation and Science Center (EROS), Souix Falls, SD.

United States Department of Agriculture (USDA). (2009), National Agriculture Imagery Program (NAIP) information sheet. Aerial Photography Field Office, Salt Lake City, UT.

Vaccari, S., van Leeuwen, M., Calders, K., Coops, N.C. and Herold, M. (2013), Bias in lidar-based canopy gap fraction estimates. *Remote Sensing Letters, 4*(4), 391-399, doi: 10.1080/2150704x.2012.742211.

Varhola, A., Coops, N.C., Bater, C.W., Teti, P., Boon, S. and Weiler, M. (2010), The influence of ground- and lidar- derived forest structure metrics on snow accumulation and ablation in disturbed forests. *Canadian Journal of Forest Research, 40*(4), 822-826, doi: 10.1139/X10-008.